A SINGLE-SIDED ACCESS SIMULTANEOUS SOLUTION FOR ACOUSTIC WAVE SPEED AND SAMPLE THICKNESS FOR ISOTROPIC MATERIALS OF PLATE-TYPE GEOMETRY

A Thesis Presented to the Faculty of the Graduate School
University of Missouri-Columbia

In Partial Fulfillment
Of the Requirements for the Degree

Masters of Science in Mechanical and Aerospace Engineering

---

by
BRETT A. RINKER

Dr. Steven P. Neal, Thesis Supervisor

May 2006

The undersigned, appointed by the Dean of the Graduate School, have examined the thesis entitled

A SINGLE-SIDED ACCESS SIMULTANEOUS SOLUTION FOR ACOUSTIC WAVE SPEED AND SAMPLE THICKNESS FOR ISOTROPIC MATERIALS OF PLATE-TYPE GEOMETRY

Presented by Brett A. Rinker

A candidate for the degree Master of Science

And hereby certify that in their opinion it is worthy of acceptance.

_____

Dr. Steven P. Neal

_____

Dr. Robert A. Winholtz

_____

Dr. Evan J. Boote

ACKNOWLEDGEMENTS

First, I wish to thank Steven P. Neal, Ph.D., for his significant guidance, instruction, and patience, without which this work would not have been possible. He has faithfully committed himself to the role of advisor in this research and has taught me a great deal. He has inspired me in my career path and I am very grateful.

Additionally, the author wishes to thank Eric Jamieson, of Honeywell Federal Manufacturing & Technologies, for his technical assistance and mentorship. He has assisted me in this endeavor and my education in nondestructive testing. He has become a good friend.

To my family, for their sacrifice and encouragement, thank you. I am eternally grateful.

Most of all, I thank my wife Tessa. You are my consistent supporter, chief advisor, and best friend. You are a constant source of joy and pride. I share this with you and dedicate it to you.

TABLE OF CONTENTS

LIST OF SYMBOLS

BSR	Back Surface Reflection
c	Speed of sound propagation
FSR	Front Surface Reflection
MHz	Megahertz
mm	Millimeter
NDE	Nondestructive Evaluation
s	Specimen
t	Time
w	Water
z	Distance in the z-direction

LIST OF FIGURES

LIST OF TABLES

A SINGLE-SIDED ACCESS SIMULTANEOUS SOLUTION FOR ACOUSTIC WAVE SPEED AND SAMPLE THICKNESS FOR ISOTROPIC MATERIALS OF PLATE-TYPE GEOMETRY

Brett A. Rinker

Dr. Steven P. Neal, Thesis Supervisor

ABSTRACT

In ultrasonic nondestructive evaluation, acoustic waves are used to inspect and characterize materials. Two commonly measured parameters are material thickness and acoustic wave speed in the material. These parameters are related through the common relationship speed equals distance divided by time. The simultaneous wave speed and thickness estimation problem arises when neither the wave speed nor thickness (propagation distance) is known. This thesis presents the initial research completed to evaluate a new solution to the simultaneous acoustic wave speed and thickness estimation problem for isotropic materials of plate-type geometry. The approach is unique in that it is implemented using one single-element transducer with only single-sided access to the material. Models are developed which show that the problem can be solved by introducing a second equation related to field perturbation. The approach is implemented using non-classical ultrasonic measurements (made with existing equipment) along with original analysis software based on the model development. Experimental results are presented in time and frequency, for metallic and non-metallic materials, and for a layered geometry. Results show that wave speed and thickness estimates determined using the new approach compare favorably with classical estimates.

I. INTRODUCTION

In the field of ultrasonic nondestructive evaluation (NDE), ultrasonic sound waves are used to inspect and measure material characteristics and conditions. Two commonly measured material characteristics are the thickness of the material and the speed of sound propagation (wave speed) in that material. Wave speed estimation is often completed for the purpose of material characterization, such as material identification or porosity detection. While thickness estimation can be used for metrology purposes, to evaluate adequacy of the material condition to meet design criteria. For example thickness measurement can inspect for material loss due to corrosion.

Estimation of either wave speed or material thickness is defined by the known relationship of speed equals distance divided by time. Time in this relationship is the propagation time required by the sound to travel through the material, from the front surface of the material to the back surface. In typical ultrasonic testing, the propagation time is measured and used along with a known material characteristic, the speed of sound propagation or the material thickness, to estimate the remaining variable. Either case is a simple one equation and one unknown relationship.

However, if both the speed of sound propagation and the material thickness are unknown, one equation and two unknowns result. This condition is known in the NDE community as the simultaneous wave speed (velocity) and thickness estimation problem. The problem is easily solved given access to both sides of the sample. Given only single-sided access, the problem becomes much more difficult.

The simultaneous wave speed and thickness estimation problem can be separated into cases where dual-sided access to the material is possible and those with only single-sided access. The dual-sided access problem can be solved using various through-transmission substitution schemes *Fei et. al.* [1.1]. Maev formulated a through-transmission approach for application to acoustic microscopy which involves the use of an axial scan to find the transducer separation that yield the peak response with and without the sample in the sound path *Maev et. al.* [1.2]. The single-sided access problem is much more difficult. The approach introduced in this thesis is a single-sided access approach applied in pulse/echo. The approach was discovered without knowledge of Maev's approach; however, the two schemes incorporate the same basic axial scan approach. In addition, solutions to the single-sided access problem have been proposed in seismology and medical ultrasound. As reviewed by Anderson et al. these approaches involve the use of multiple element transducers (or multiple transducers) and rely on either estimates of the time delays required to achieve focusing or estimates of refracted angles as a basis for wave speed estimation *Anderson et. al.* [1.3].

This thesis presents a new solution, derived at the University of Missouri-Columbia, to the simultaneous wave speed and thickness estimation problem *Neal* [1.4]. This solution employs a single element piezoelectric transducer at normal incidence to the material specimen and requires only single-sided access. The problem of one equation and two unknowns is solved by introducing a second, independent equation.

The second equation is derived from a focal law, based on diffraction phenomenon, which is routinely used to calculate the change in water path, required to move the focal zone of the spherically focused transducer from the front surface to the back surface of

the specimen. The water path is the distance in water the sound travels from the end of the transducer to the front surface of the material specimen. The new approach is executed by experimentally determining the change in water path (time shift) necessary to move the focal zone from the front surface to the back surface. Experimentally, an axial scan is used to collect the data required to determine the necessary time shift. Once the time shift is determined, it is used along with the propagation time from the front to the back surface to calculate the wave speed and thickness of the unknown material.

Following this introduction, this thesis will discuss the ultrasonic equipment used in this research, the characteristics of ultrasonic piezoelectric transducers, and traditional NDE test methods for calculating the material wave speed. This will be followed with the development of mathematical models and a presentation of the new method as it was experimentally applied to different engineering materials and test geometries. Finally, a summary of the research will be provided.

II. BACKGROUND

a. Ultrasonic Test Equipment

All ultrasonic data in this thesis was captured in a standard immersion pulse-echo configuration with the piezoelectric transducer at normal incidence to the material specimen. The specimen was placed in a water tank with a leveling table inside the tank and a set of transducer control motors mounted on top of the tank. The tank uses three servo motors designed to move the transducer in the x, y, and z directions. These motors are driven by a xyz motor controller, which is directed by the data acquisition software located on the data acquisition computer *Cepel* [2.1].

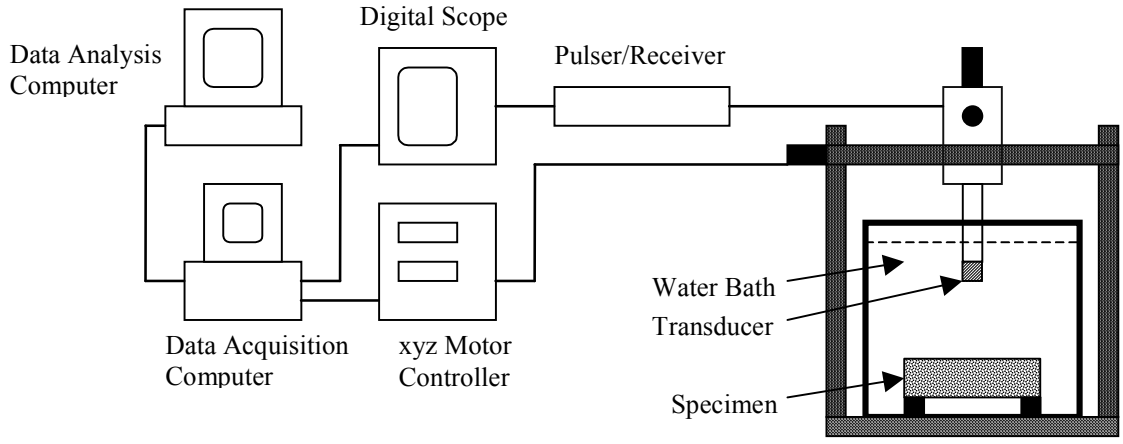

Figure 1: Ultrasonic Testing System

The data acquisition computer uses a control and oscilloscope software program written in the Labview programming language *Cepel* [2.2]. The software program converts user inputs for the desired scan geometry into transducer positional control commands, collects the ultrasonic wave form signals into a binary format, and displays the collected signals real-time on the user interface oscilloscope.

The ultrasonic wave form signals, or Radio Frequency (RF) signals, are generated with a Panametrics pulser-reciever, model 5052P/R which pulses a Panametrics piezoelectric transducer with a broadband pulse. The return signals are captured with a Gage data acquisition card with 12 bit resolution. All return signals were digitized at a 100 MHz sampling rate. At each measurement position within the scan, 64 pulses were averaged together and that average signal was recorded into the binary format data file *Cepel* [2.3].

Once the experiment is complete, the resulting data file, which includes a preamble of information describing the experimental setup, is transferred to a data analysis computer. The data analysis computer uses Matlab code, created specifically for this thesis and test method, to analyze the binary output file *Neal* [2.4]. The results of that analysis are reported in the results chapter of this thesis.

b. Piezoelectric Ultrasonic Transducers

In a pulse–echo test method, as used in this thesis, the same transducer is used for both transmission and reception of the broadband ultrasonic signal. Most ultrasonic transducers use a single piezoelectric element to transmit and/or receive ultrasonic signals. As a transmitter the transducer receives the broadband electrical pulse from the pulser-receiver and is excited by that pulse to produce the ultrasonic signal pulse. Once the ultrasonic signal is reflected from the specimen, the transducer reverses this process and acts as the receiver. When the ultrasonic return signal impacts the transducer it excites the piezoelectric element and generates a time varying electrical signal.

As the transducer transmits the ultrasonic signal into the coupling media, in this case water, diffraction effects and the physical characteristics of the piezoelectric element

create nodes in the acoustic field. Nodes are areas of constructive and destructive interference between the ultrasonic signals generated at different points across the face of the transducer. The pattern and relative size of the nodes is unique to each transducer and acts like a signature. This signature is created primarily by manufacturing and piezoelectric material variability, which combine to determine the efficiency of the transducer and to vary the location of the nodes creating a unique sound field.

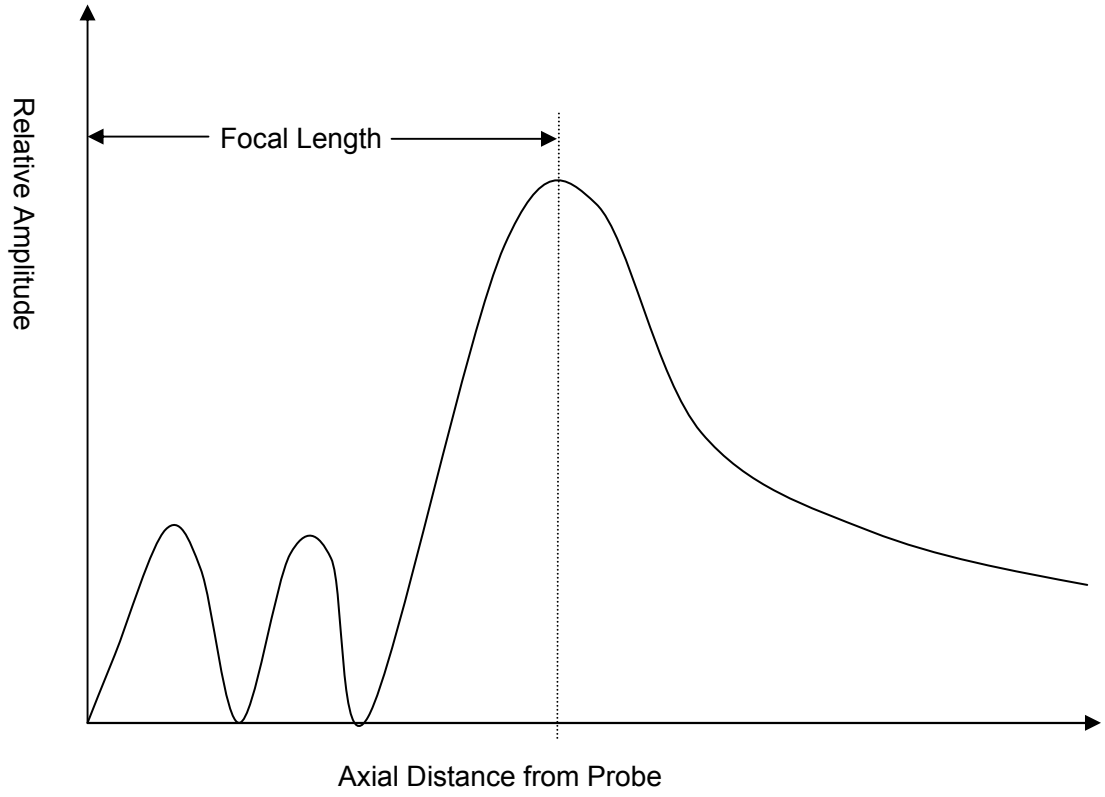

Figure 2: Illustration of a typical focused transducers axial response

In addition to being distinct identifiable features of the ultrasonic transducers unique sound field, nodes have an important effect on the ultrasonic signals response to the material specimen being evaluated. The sensitivity and resolution of the ultrasonic transducer is most effective at nodes of constructive interference, areas of high acoustic pressure. Meanwhile areas of completely destructive interference have no ability to

inspect the material specimen at that point in the transducers sound field. By using this principle, inspectors can improve the effectiveness of their tests by placing the area of interest in the media to be inspected at a node of constructive interference.

For this reason, ultrasonic transducer manufacturers produce piezoelectric transducers with the addition of a concave lens on the tip of the transducer. This creates a spherically focused ultrasonic transducer. Focusing the sound field with the use of a lens increases the magnitude of the sound pressure at the point of focus, creating an extremely prominent node of constructive interference within the sound field. This focused node improves the lateral resolution and signal-to-noise ratio of the sound field at the point of focus. The location of the focal node is defined by the focal length, which is the axial distance from the face of the transducer to the point of maximum focus in a specified medium, typically water. Due to diffraction effects the focal length of the transducer is different in different materials, but the point of maximum focus is always present.

c. Classical Ultrasonic Velocity Estimation

In a classical single-sided velocity of sound propagation estimate, the thickness of the material specimen, z_s, is known. The specimen is placed in the water tank with the transducer at normal incidence in a pulse-echo configuration. The single ultrasonic transducer sends the RF-signal into the material specimen and collects the waveform reflections from the front and back surfaces.

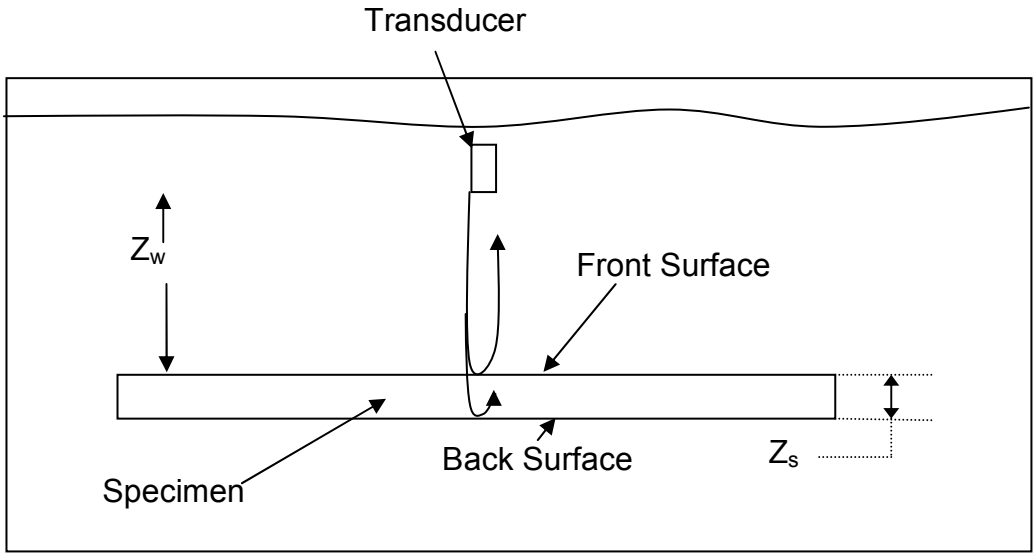

Figure 3: Illustration of Classical Velocity Estimation

With the ultrasonic signal collected, the propagation time from the absolute maximum of the front surface reflection to the absolute maximum of the back surface reflection, Δt_s, is measured as shown in Figure 4. Other methods of measuring Δt_s include measuring the propagation time between the first and second back surface reflections, and using the first deviation of a waveform from the noise to break a given threshold. However, for the purposes of this thesis the front and back surface absolute maximum response is used.

The equation for the velocity of sound propagation in the material, c_s, is defined as,

$$c_s = \frac{z_s}{\Delta t_s} \qquad [1]$$

With each of the required variables known, the wave speed estimation can be completed. However, if the thickness of the material specimen is unknown, the problem becomes more complex.

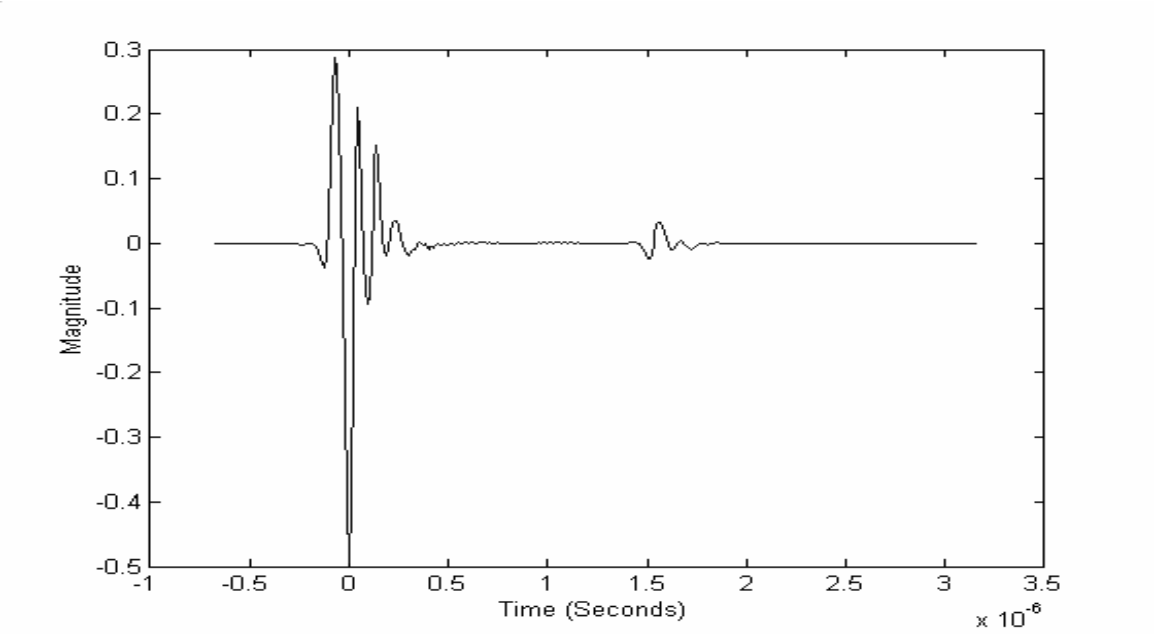

Figure 4: A typical rf-signal and the measurement of Δt_s

III. EXPERIMENTAL PROCEDURES

a. General Procedures & Setup

Throughout the experiments completed for this thesis, several operations were conducted prior to each experiment. These experimental procedures are standard for many pulse-echo immersion test configurations. Therefore, to reduce repetition in later chapters of this thesis, these procedures will be mentioned only within this chapter and ignored in later chapters of this thesis.

Once the material specimen to be examined has been selected, its thickness was physically measured with hand calipers, to allow a classical wave speed measurement to be completed in the future. The specimen and transducer are then inserted in the water tank below the waterline. With the specimen and transducer in the tank they are examined for the presence of air bubbles on their surfaces and swept clear as necessary. Air bubbles on the lens of the transducer would impede consistent signal transfer to the water. Likewise, air bubbles on the material specimen surface reflect back false front surface reflections and impede signal transmission into the material.

The axis of sound propagation is adjusted to ensure perpendicularity of the ultrasonic transducer to the front surface or the material specimen. This process is completed in two phases. First, the table in the bottom of the water tank, which holds the material specimen, is adjusted until the front surface of the specimen is level. This is performed by moving the transducer in both the x and y directions, and adjusting the legs of the table until the front surface reflection (FSR) is stable, in time, on the oscilloscope. Second, the ultrasonic transducers axis of sound propagation is aligned to normal

incidence, by adjusting the transducer support gimbals while observing the oscilloscope. The ultrasonic transducer and material specimen have achieved normal incidence when the front surface reflection is both earliest in time and maximized in amplitude.

Next adjustments to the pulser-receiver are performed to properly digitize the waveforms of interest. The goal of proper signal digitization is to maximize the signal collected by the data acquisition card without the signal becoming saturated. This reduces the effects of digitization by using most of the 12 bits of available resolution for the largest signal of interest, in most cases the front surface reflection. By more accurately digitizing the waveform the best case for future data analysis is created.

Since the experiments for this thesis involve multiple water path lengths, which will be defined in later sections of this chapter, and longer water path lengths attenuate the rf-signal more extensively, it is important to position the transducer at the shortest path prior to adjusting the settings on the pulser-receiver. For this thesis, the damping, high pass filtering, and repetition rate controls were adjusted to their mid range values on the pulser-receiver and left alone for each experiment. To complete the signal optimization the amplifier gain on the pulser-receiver was then increased until the largest signal of interest was approximately 90% of full scale, unless saturation effects required a lower gain setting.

The attenuation effects of some of the material specimens used in these experiments are significant enough that when the front surface reflection is properly digitized the back surface reflection (BSR) does not use up an adequate portion of the available resolution. This is especially true with longer water path lengths when the attenuation effects of water are maximized. To compensate for this phenomenon a second scan was completed

which properly digitizes the back surface reflection using the same approach as previously discussed. This will be discussed further in later portions of this thesis, but by combining these two optimized scans the accuracy of the data analysis calculations was improved.

The final experimental preparation steps before the ultrasonic scan is initiated include a measurement of the water temperature and a classical velocity of sound propagation measurement. The water temperature within the tank is measured and the value is entered in the data acquisition software *Cepel* [3.1]. This allows the data analysis software to accurately calculate the velocity of sound propagation in the water. Finally, the classical velocity measurement is completed as described previously. This is performed as a baseline for comparison of the estimations the new test method generates.

b. Classical scan geometry

For the purpose of clarifying future discussions, this section will define a few traditional ultrasonic scan geometries which will be used in this thesis.

i. 2D Raster Scans

The two dimensional raster scan is traditionally used to evaluate a planar area of interest in a material specimen. The scan is completed by moving the ultrasonic transducer in a grid pattern in the x and y directions, parallel to the front surface of the material specimen. The grid is completed parallel to the front surface of the specimen, so that the front surface reflection always occurs at the same propagation time. The propagation time at which the front surface reflection occurs for this raster scan is defined as its water path time.

ii. Axial Scans

When a new transducer is purchased for immersion ultrasonic testing the user will typically complete an axial scan to characterize the sound field of the transducer. An axial scan is completed by aligning the transducer above the reflector, specimen, and making measurements at several water paths in the z-axis. By recording the amplitude of the ultrasonic transducers response at each water path, as previously depicted in Figure 2, the characteristics of the transducers sound field such as axial nodes and the focal length, where appropriate, can be identified.

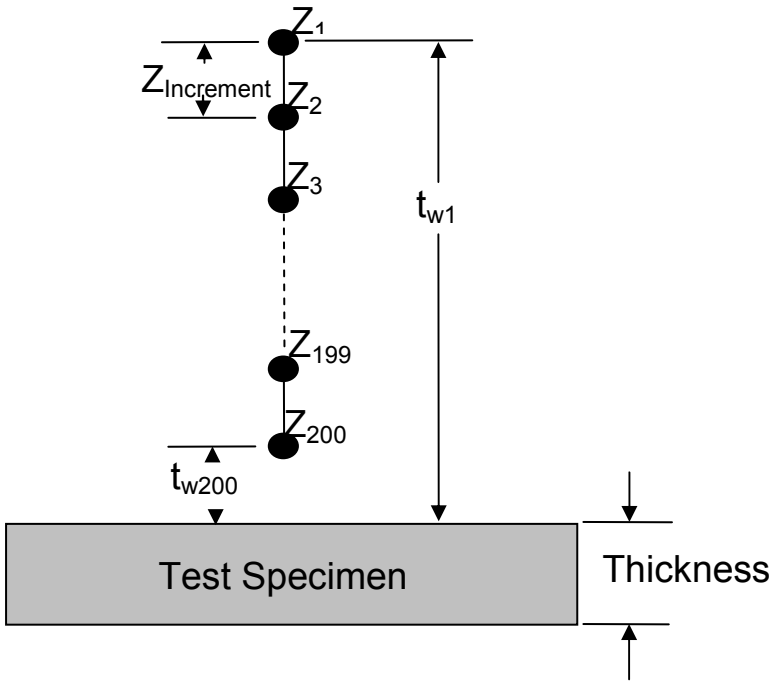

Figure 5: Illustration of axial scan geometry

iii. Three Dimensional Raster Scans

Most of the experiments completed to evaluate the new experimental test method presented in this thesis use a hybrid of the two previous scan geometries. In the three dimensional raster scan, a two dimensional raster is completed at a series of water paths resulting in a matrix of data including transducer location as well as the return rf-signal. This scan geometry would traditionally be used to inspect a volume of the specimen for defects in the material. By moving the focal node, when a spherically focused transducer is used, throughout the specimen the most rigorous inspection of the material is achieved.

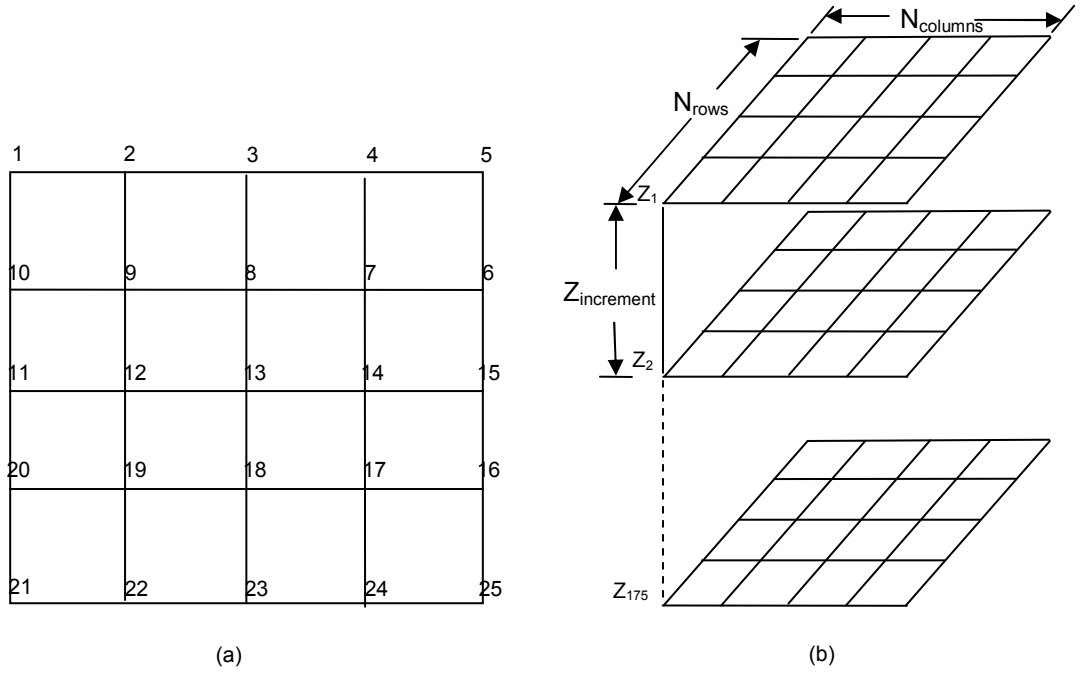

Figure 6: Illustration of the 3 Dimensional raster scan geometry

IV. SIMULTANEOUS VELOCITY AND THICKNESS APPROACH

a. Models (equations)

The goal of this thesis is to evaluate a simultaneous solution for thickness and the acoustic velocity in an unknown isotropic material of plate type geometry using only single sided access to the material specimen. As discussed previously, and defined in equation [1], the velocity of sound propagation in a media, c_s, is a function of both the time the sound travels in the specimen, Δt_s, and the specimen thickness, z_s. While the propagation time in the specimen can easily be measured, as shown in figure 4, the thickness of the specimen is difficult to measure in configurations where only single sided access to the specimen is available. This leaves a single equation with two unknown variables.

The premise behind the new simultaneous approach is to use the characteristic response of an ultrasonic transducers sound field to solve for one of the unknown variables *Neal* [4.1]. By moving a feature of the transducers response through the material specimen, from the front surface to the back surface, the water path position where the transducers response feature interacts with the signals of interest can be measured. In this thesis, a spherically focused broadband transducer was used and the focal node was the transducers sound field characteristic which was moved through the specimen. However, this method could be completed with a non-focused transducer and any sound field node as well.

If z* is defined as the point of maximum response in the transducers sound field, then it can be expressed as shown in equation [2]. For the spherically focused transducer z*,

$$z^* = \int_A c(x, y, z)dxdy \qquad [2]$$

in water, is equivalent to the focal length of the transducer. Therefore by moving the transducer to a water path equivalent to the focal length, the transducers point of maximum response to the front surface reflection (FSR) is found.

Finding the point of maximum response for the back surface reflection (BSR) is more complicated. This research is only applied to isotropic materials of plate type geometry so no lensing of the sound field occurs. However, z* is a function of the velocity of sound propagation, which alters the effective focal length of the transducer as the rf-waveform enters the specimen. This phenomenon is referred to as diffraction effects, depicted in Figure 7, and results from changes in wavelengths due to the change in sound propagation speeds.

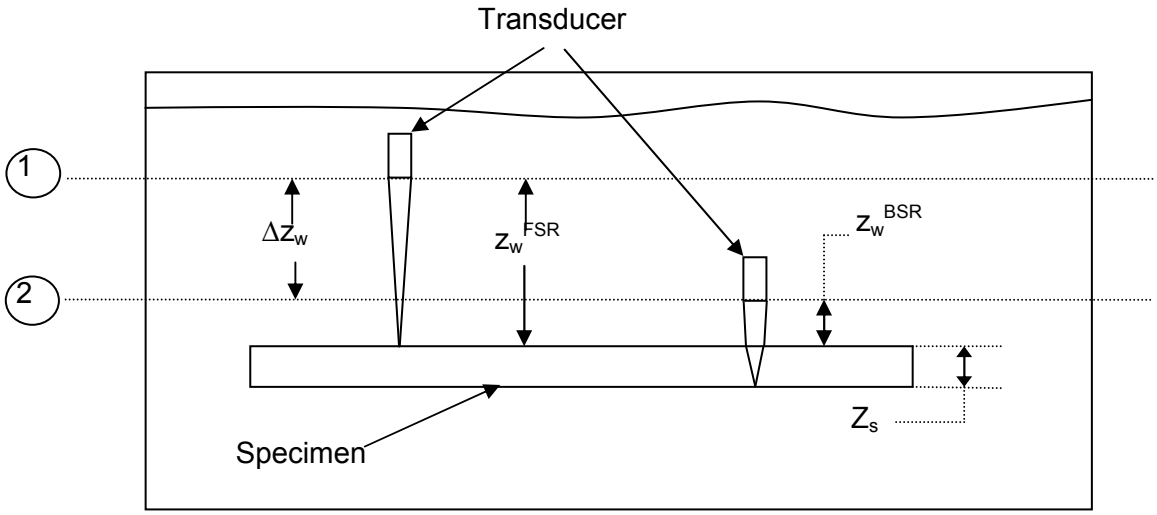

Figure 7: Illustration of transducers at water paths of maximum response

If the transducers sound field is used in a material with a higher wave speed than water, then the wavelength is shortened and the sound field characteristics are compressed, effectively reducing the focal length of the transducer. The compression of the sound field is solely a function of the shift in wavelength and is expressed

mathematically in equation [3]; where z_1 and z_2 are the focal lengths of the transducer in the respective materials.

$$c_1 z_1 = c_2 z_2 \quad [3]$$

However, in the case where the sound field is focusing in the material specimen, the sound must pass through the both a water path length of water and a distance in the specimen. If the specimen and the water are assumed to each possess unique speeds of sound propagation, equation [3] for this test geometry would be expressed as:

$$c_1 z_1 = c_1 z_2 + c_3 z_3 \quad [4]$$

This expression can be simplified as follows:

$$z_1 = z_2 + \left[\frac{c_3}{c_1}\right] z_3 \quad [5]$$

Returning to the problem of simultaneous velocity and thickness estimation as depicted in Figure 7, equation [4] is expressed for both the FSR and BSR focused conditions and becomes:

$$z^* = z_w^{FSR} = z_w^{BSR} + \frac{c_s}{c_w} z_s \quad [6]$$

Solving for one of the unknown variables c_s yields:

$$c_s = c_w \left[\frac{z_w^{FSR} - z_w^{BSR}}{z_s}\right] \quad [7]$$

Since the difference in the water paths z_w^{FSR} and z_w^{BSR} is equal to the product of the wave speed in water and the difference in water path times, equation [7] can be expressed further as:

$$c_s = c_w \left[\frac{\Delta z}{z_s}\right] = c_w \left[\frac{c_w \Delta t_w}{z_s}\right] \quad [8]$$

Finally if equation [1] is solved for the specimen thickness, c_s, and substituted into equation [8] the relationship becomes:

$$c_s = c_w \left[\frac{c_w \Delta t_w}{c_s \Delta t_s} \right] \qquad [9]$$

this simplifies to yield:

$$c_s = c_w \sqrt{\frac{\Delta t_w}{\Delta t_s}} \qquad [10]$$

For equation [10], the wave speed of water, c_w, is known, the propagation time in the specimen, Δt_s, can be measured, and Δt_w, the time shift, is a function of the experimentally measured quantities z_w^{FSR} and z_w^{BSR}. The only remaining unknown is the wave speed in the specimen, c_s. Once the velocity of sound propagation is calculated with equation [10], it can be used to determine the thickness of the unknown media using the original expression, equation [1], which now only has a single unknown variable.

The same experimental technique can be applied to any set of waveforms *Neal* [4.2]. In the case of a layered material specimen, as depicted in Figure 7, the sound waves must past through the water path length, the thickness of the first layer of the specimen and the layer to be inspected. If equation [4] is rewritten to reflect the geometry illustrated in Figure 7, the following expression results:

$$c_w z_w^{Int} + c_{s1} z_{s1} = c_w z_w^{BSR} + c_{s1} z_{s1} + c_{s2} z_{s2} \qquad [11]$$

This simplifies to the expression:

$$c_w z_w^{Int} = c_w z_w^{BSR} + c_{s2} z_{s2} \qquad [12]$$

This result shows that the solution for the second material layer is independent of the characteristics of the first layer. Therefore, this characterization method can be used for

any set of signals in an unknown material, with no prior knowledge of the surrounding environment, except for the coupling media.

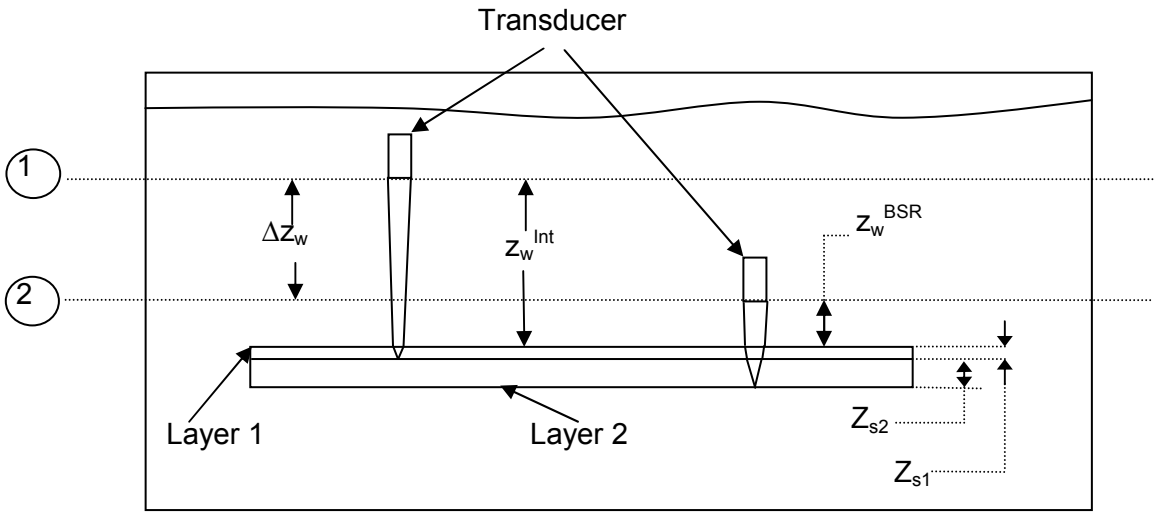

Figure 8: Illustration of transducers at water paths of maximum response for layered media

b. Implementation

With all of the experimental preparation completed, as discussed in the previous chapter, the data collection and estimation is ready to be completed. All experiments in this thesis were completed with either axial or three dimensional raster scans. The discussion in this section is interchangeable for either axial or 3D raster scans except where noted. The major differences in the approaches include the amount of data taken and the number of estimates and averaging completed.

The final step before starting the scan is to position the ultrasonic transducer; in this case a 15 MHz spherically focused broadband transducer with a three inch focal length in water, at a pre-FSR focused water path. In the discussion in the previous section, the equations and illustrations showed the transducer positioned at the precise water paths of focus for both the FSR and the BSR. Given that the motivation for this test method is that the material characteristics are unknown, choosing the two precise water paths is

unlikely and time consuming. Therefore the experimental scans are initiated with the transducer aligned in a pre-focused state for the FSR waveform, with the transducer focused in the water. The data acquisition software is then programmed by the user to collect enough water paths of data to characterize most of the transducers focal length *Cepel* [4.3]. The scan is completed with the transducer face near the surface of the specimen without moving close enough to generate interference effects. If after completing the scan and analyzing the data the range of water paths was found insufficient to include the water paths of maximum response for the FSR and BSR, then a transducer with a longer focal length would be necessary.

Once the scan is completed, the data for the experimental setup is stored in the preamble of the data file as well as the recorded signal at each measurement position. The rf-waveforms recorded at each measurement position are stored in a three dimensional matrix format, with the matrix dimensions equivalent to the number of raster positions by the number of water paths by the length of the recorded rf-waveforms. For example, a three dimensional raster scan of 200 data point wave forms, in time, with a 5x5 raster completed at 100 water paths, would produce a data matrix with the dimensions 25x100x200. The data analysis Matlab programs written for this research use the preamble data as well as the waveform data matrix to calculate the estimates of the velocity of sound propagation and the thickness of the material specimen *Neal* [4.4].

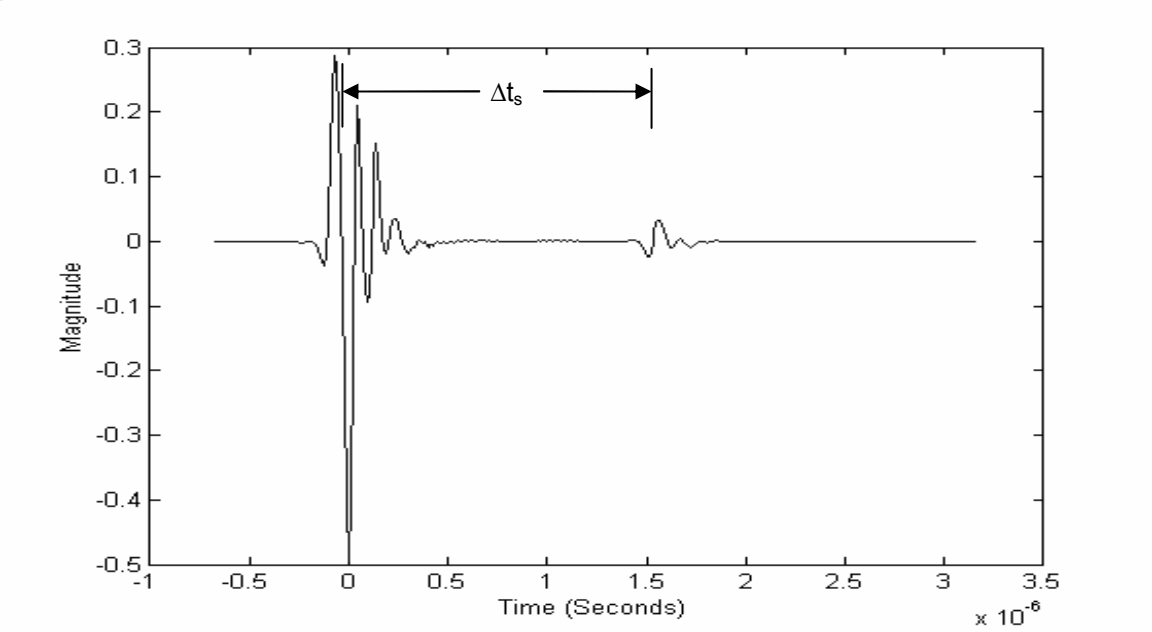

Figure 9: Typical rf-signal generated by the ultrasonic scan

With the data file opened and loaded by the data analysis software, the program aligns the FSR of each signal in the rf-waveform matrix. The point of absolute maximum response in the FSR for the waveform at each measurement position is identified and offset such that the FSR occurs at the same position in the data string for all signals. This improves data analysis, by placing the FSR, and thus the BSR, consistently in the same data windows as well as improving the appearance of the resulting graphical figures. Additionally, the offset of each FSR is used to create a matrix of water path times using information from the data files preamble. The result as shown in Figure 9 is each wave form in the matrix has the absolute maximum response of the FSR signal placed at time zero.

The next step in the data analysis was to isolate the FSR and BSR for each measurement position. Isolation was completed by a combination of user inputs and the application of Gaussian windows to eliminate any signals that are not of interest. By creating a matrix for both the FSR and BSR, and multiplying the amplitudes of each

signal by a Gaussian window centered on absolute maximum response, any signals outside of the window are eliminated and the signal is shaped such that the points of absolute maximum response are easily identified. The aligned signals, Gaussian windows, and resulting signals for both the FSR and BSR are shown in Figure 10.

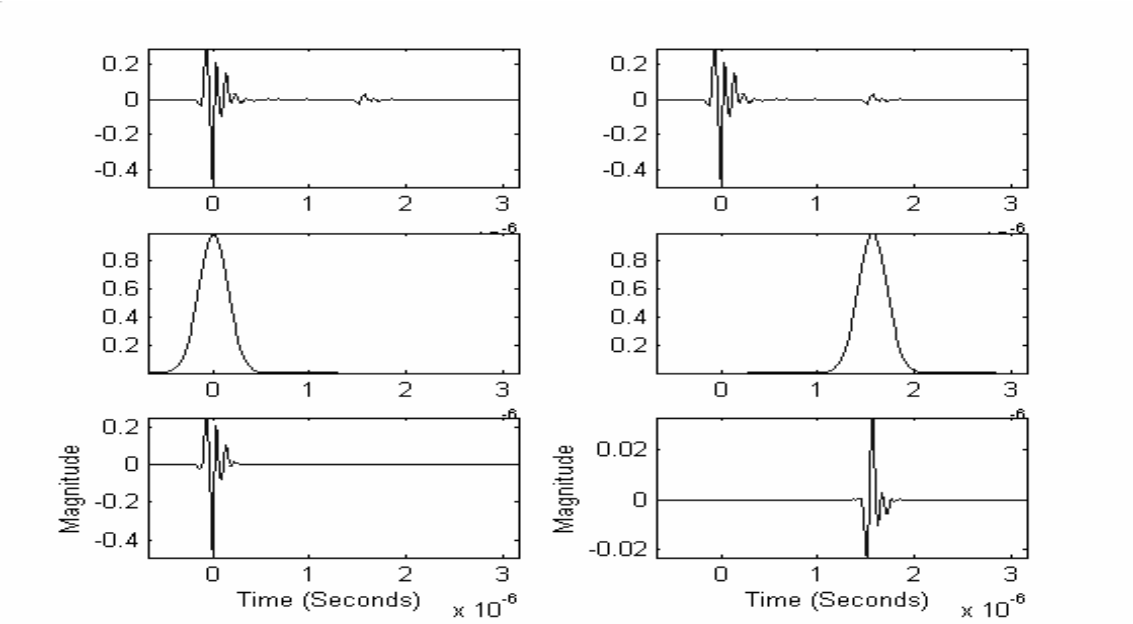

Figure 10: Rf-signals with Gaussian multipliers and resulting signals (FSR signal on left with BSR on right)

Finally, with the FSR and BSR signal matrices prepared, the software is ready to calculate the material characteristics. Figure 11 is a normalized summation of the FSR and BSR matrices that result from the data preparation. To complete the estimates the water path of absolute maximum responses for both the FSR and BSR are identified *Neal* [4.5]. This response was correlated to the water path time where each maximum occurred, as depicted in the previous sections equations and illustrations. The difference in water path time from the FSR maximum to the BSR maximum responses can then be calculated and input into equation [10]. The resulting speed of sound propagation is then input into equation [1], as previously discussed, to calculate the specimen thickness.

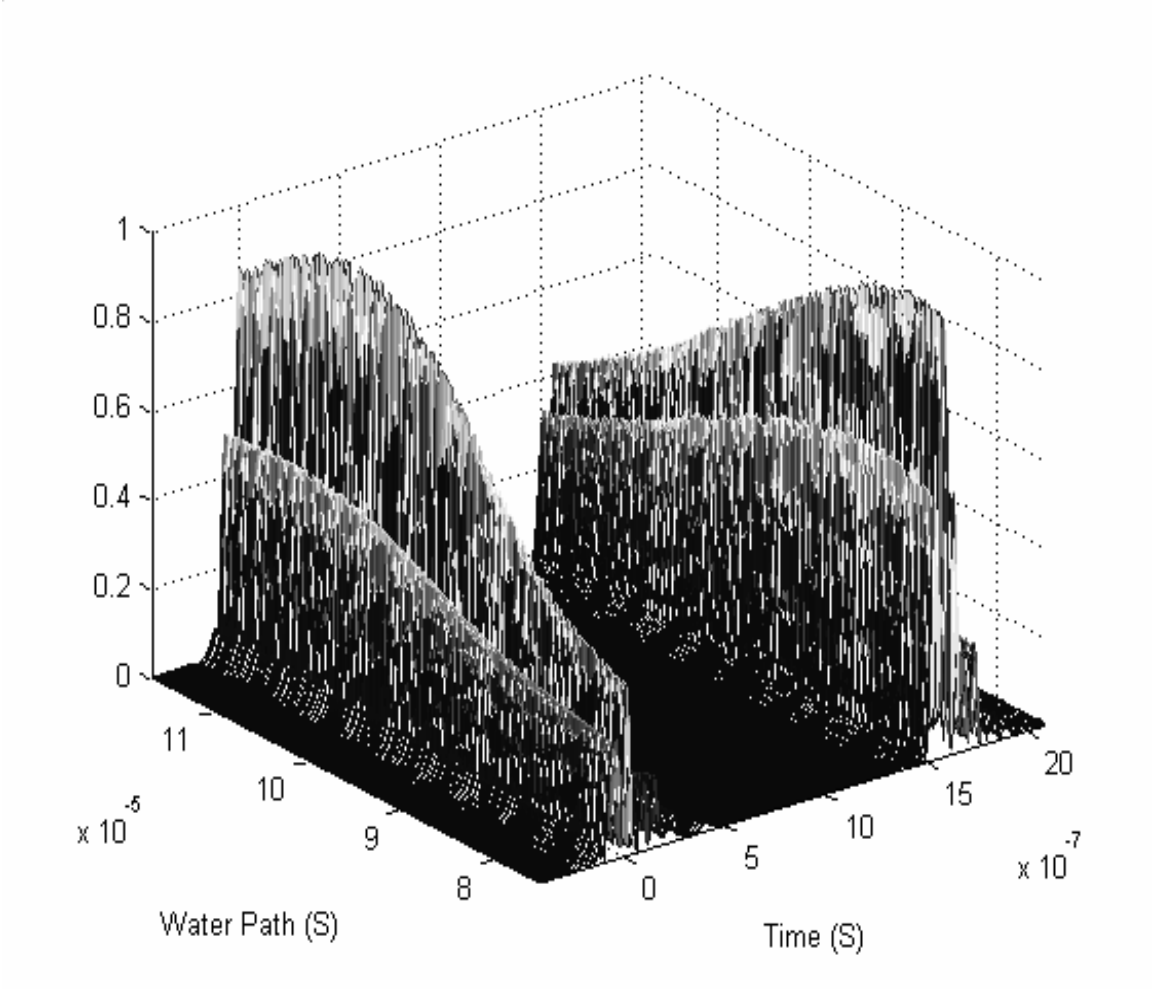

Figure 11: Transducer response (normalized and absolute) as a function of water path and time

c. Frequency Domain Implementation

Until this point in the thesis, all calculations have been completed in the time domain. However, by using the fft (fast Fourier transform) command in Matlab, the data can be converted into the frequency domain as well. Performing the measurements in the frequency domain allows more information to be gathered about the material. For example, the extent of high frequency attenuation and the presence of any frequency dependence to the material characteristics being measured. Due to these advantages, all of the experiments presented in this thesis were analyzed in the frequency domain, while only a few were completed in the time domain.

To complete the material characterization in the frequency domain, the experimental setup, scan, and much of the data analysis was performed as previously described. The deviation from the time domain procedure occurs after the Gaussian windows are applied to the aligned data and both the FSR and BSR waveform matrices are created. Once this is complete the Matlab fft command is used, transferring each matrix and the included signals into the frequency domain. The resulting frequency domain matrices are shown graphically in Figure 12 and Figure 13.

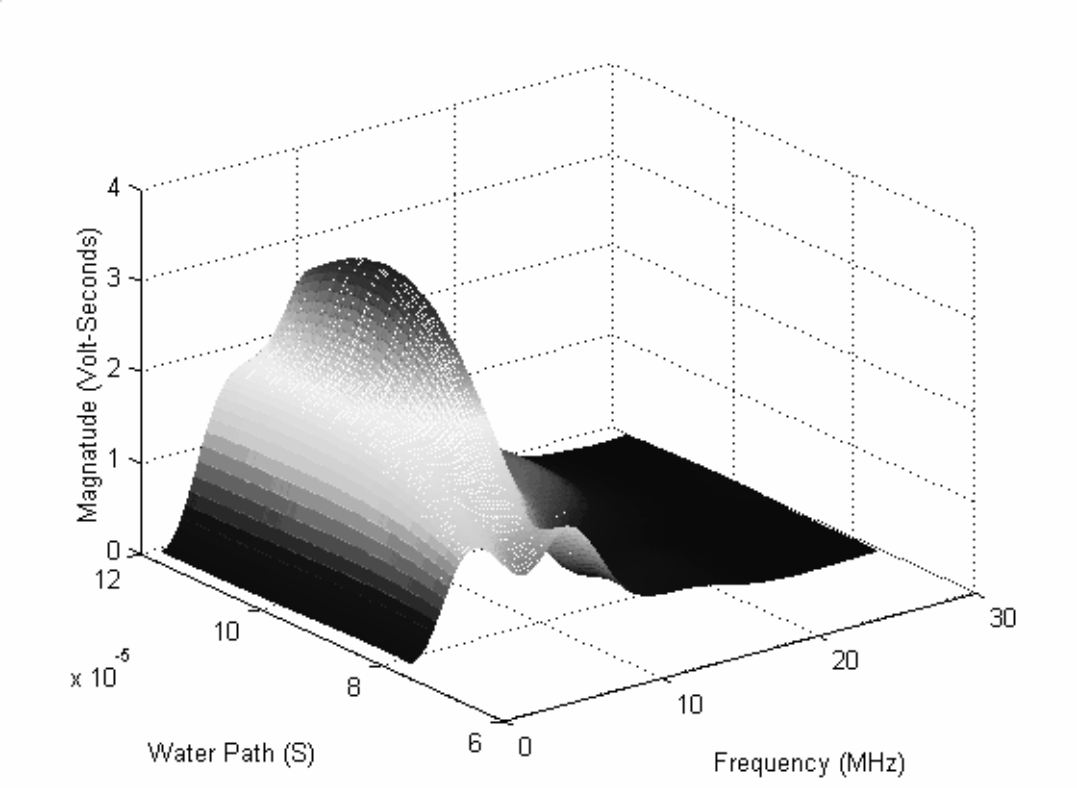

Figure 12: FSR Transducer response (absolute) as a function of water path and frequency

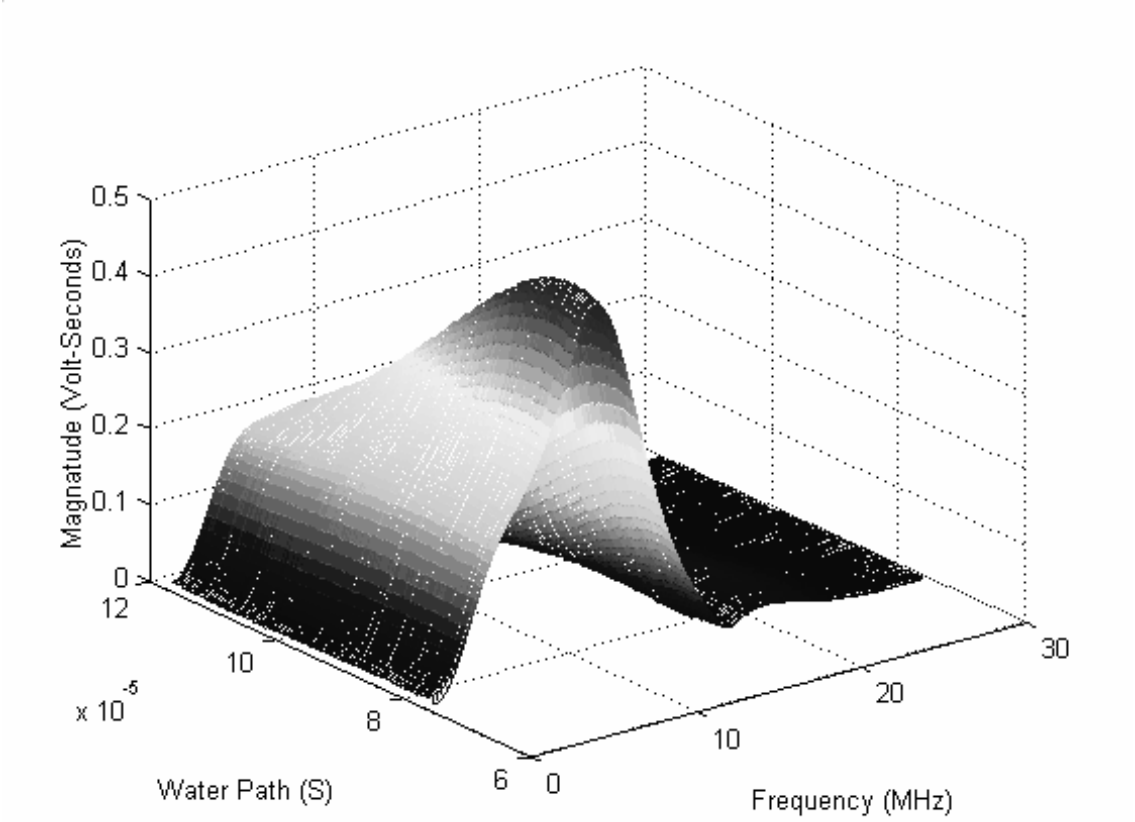

Figure 13: BSR Transducer response (absolute) as a function of water path and frequency

By observation of Figure 12 and Figure 13, it is determined that while the transducer is driven broadband with a center frequency of 15 MHz, not every frequency has shown a strong response to the material specimen. In fact, the center frequency of the response is approximately two thirds the center frequency of the original pulse produced by the transducer. The variation in response is due to the both the initial excitation of the transducer and the attenuation effects of the water and material specimen. Therefore, a range of frequencies which presents a moderate to strong response is selected by the data analysis software user and the calculations are completed only for that specified range.

Once the frequency range of interest is selected, the software creates a polynomial fit through the data for each frequency across all water paths. The curve fit allows for

interpolation between the water path data points for a more accurate estimation of the water paths of absolute maximum response. Figure 14 displays the normalized curve fit at one frequency for both the FSR and BSR along with every tenth water path data point. Figure 15 presents the same polynomial curve fits without the water path data points or the normalization. The difference in the amplitudes of the fits is due to attenuation of the sound waves as they pass through the material specimen. Less attenuative materials will produce a smaller difference in waveform amplitude.

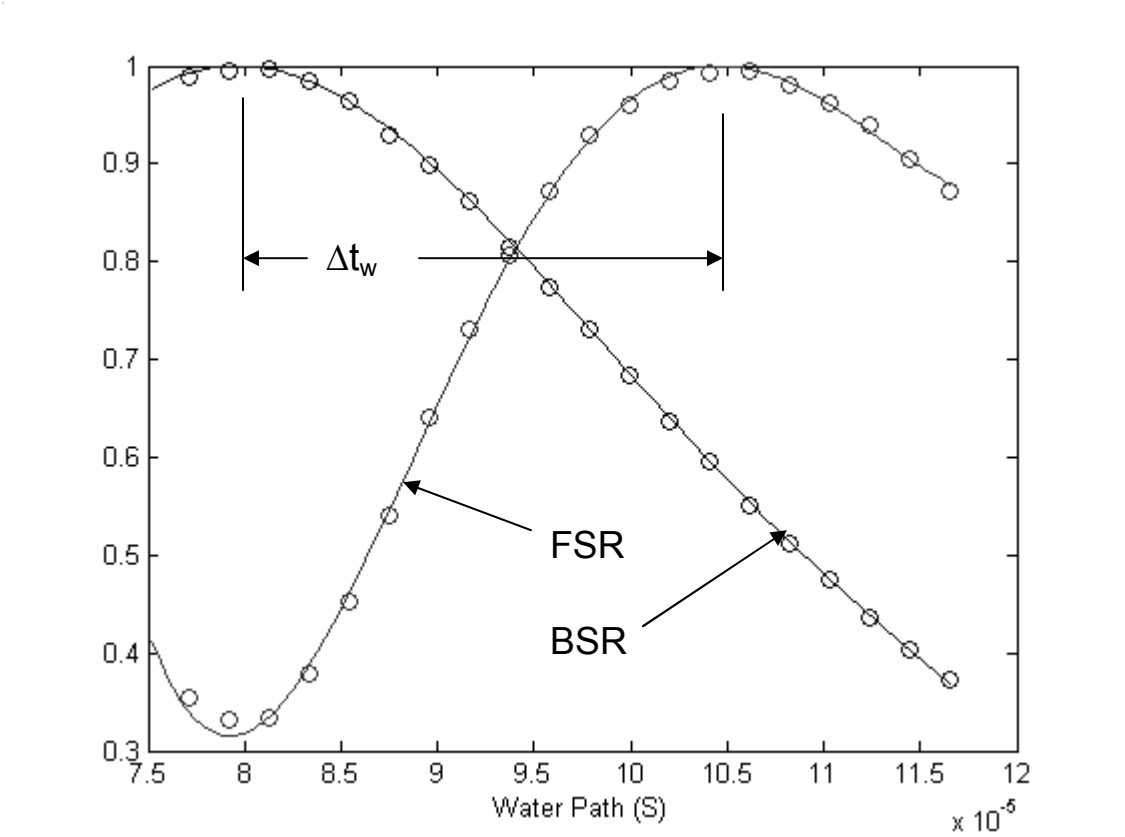

Figure 14: Resulting normalized curve fits through water path data points for a single frequency

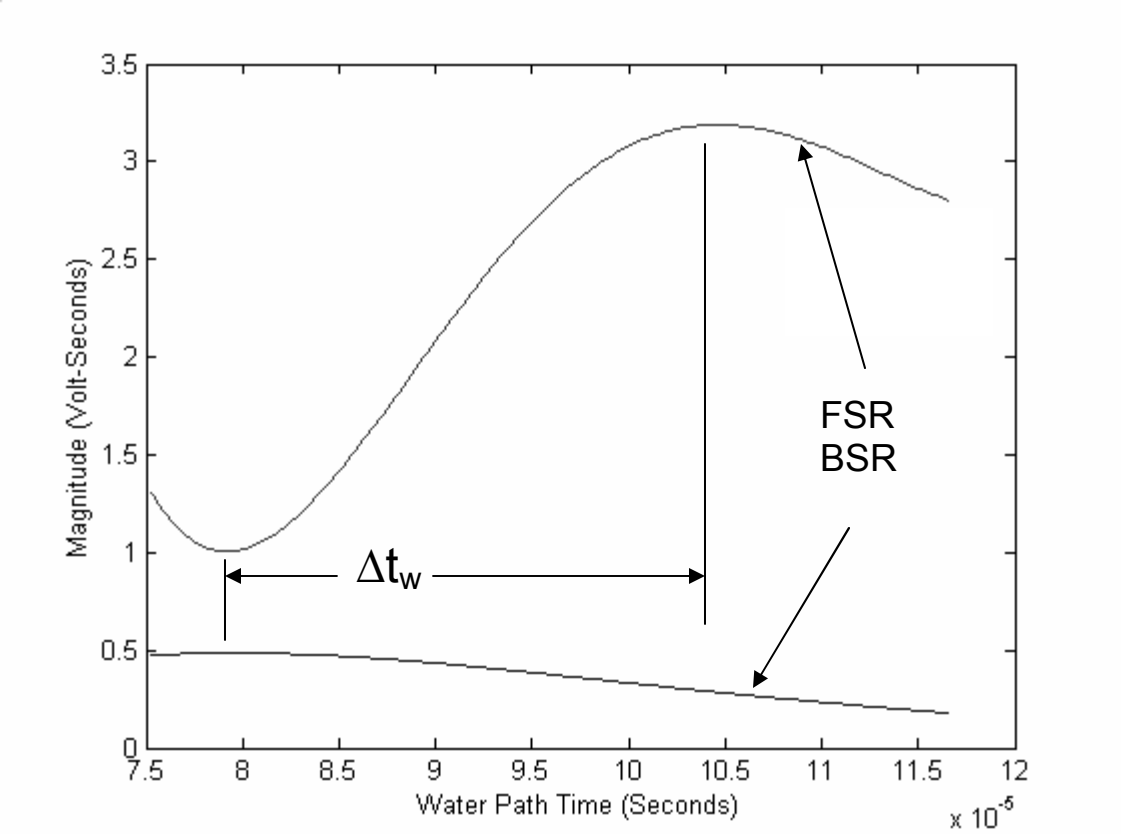

Figure 15: Calculated curves for FSR and BSR at a single frequency (without water path data points)

Finally, the water path times of maximum response for the FSR and BSR are identified for each frequency in the selected range. Calculation of the difference in water path times at each selected frequency is completed and used in equation [10]. The velocity of sound propagation to be calculated is reported as a function of frequency. Since all of the material specimens used in this research are non-dispersive, the water path times and thus the velocity estimates are effectively constant for all frequencies, as shown in Figure 16.

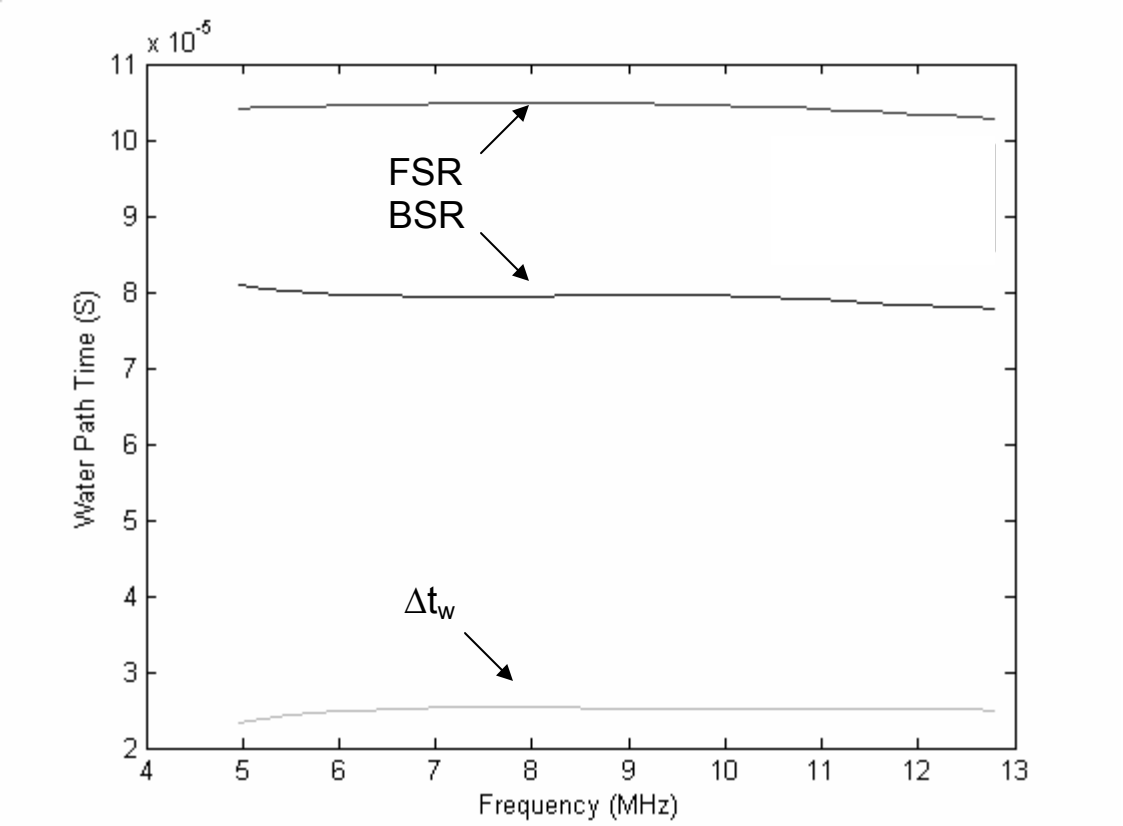

Figure 16: Water path times of maximum response as a function of frequency

V. RESULTS

In this chapter, the execution of the new simultaneous estimation method in unique four experiments will be discussed. Each experiment will examine different approaches to applying the new characterization method *Neal* [5.1]. Additionally, each experiment uses a different material specimen and the analysis results for each will be presented.

a. Single Axial Scan Experiment

This experiment evaluates the simplest sample and test geometry, the axial scan with a homogeneous material specimen. The material specimen selected was a piece of steel plate of known geometry. Prior to completing the ultrasonic axial scan, a classical velocity of sound propagation and thickness measurement was completed. As described previously, the thickness was measured physically with hand calipers, which was followed by the velocity measurement. The results of classical measurements are shown in Table 1.

Table 1: Classical measurement results for the single z-scan

Thickness (cm)	Δt_s (μs)	c_s (cm/μs)
0.47498	1.5920	0.5967

With the classical evaluation complete, an axial scan was performed with the 15 MHz broadband spherically focused transducer. The scan consisted of 200 water paths with a spacing, $Z_{increment}$, of 0.1513 mm as previously depicted in Figure 5. This scan covered enough water path distance to move from the pre-focused FSR condition to the post-focused BSR condition. While this convention of starting away from the specimen and moving closer with each increment was used for each experiment in this research, the

reverse could also be performed with no effect on the data analysis. Therefore, in the data presented in this thesis, water paths of greater time occur earlier in the scan.

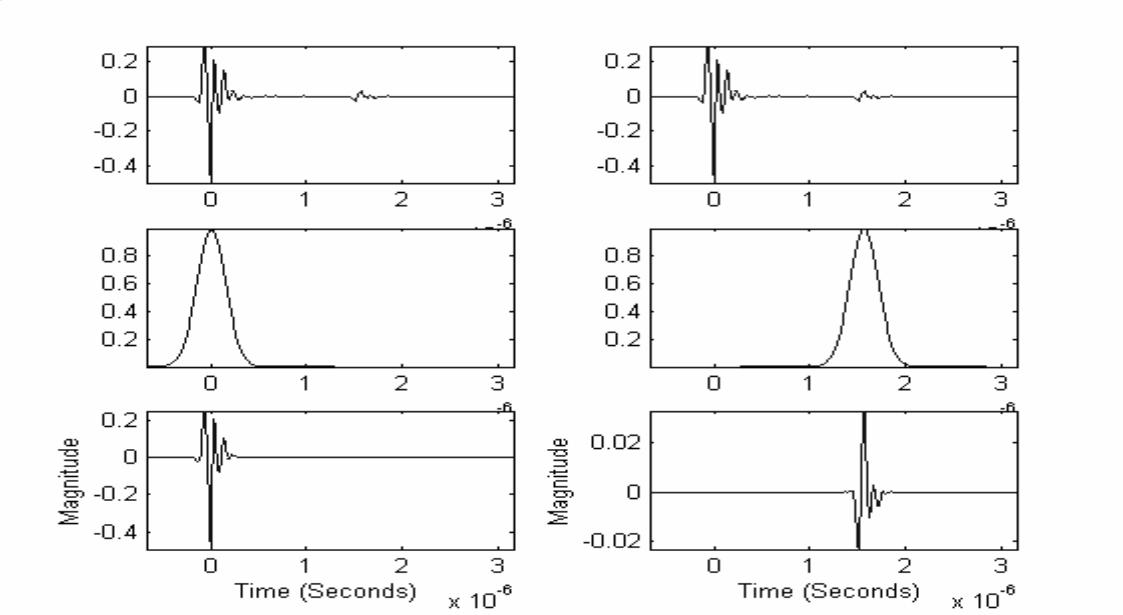

Figure 17: Axial Scan sample aligned rf-signal with Gaussian multiplier and resulting signal (FSR signal on left with BSR on right)

Once the scan was completed, the data was prepared for analysis by aligning the waveforms and applying the Gaussian multiplier windows, as discussed previously and depicted in Figure 17. Data analysis was initially completed in the time domain *Neal* [5.2]. Due to the extensive attenuation of the BSR signal from to traveling through the steel specimen, as observed in Figure 17, the FSR and BSR signals were normalized for improved graphical presentation as shown in Figure 18. Evaluation of this image shows that the axial scan completely covered the water paths of maximum response for both the FSR and BSR.

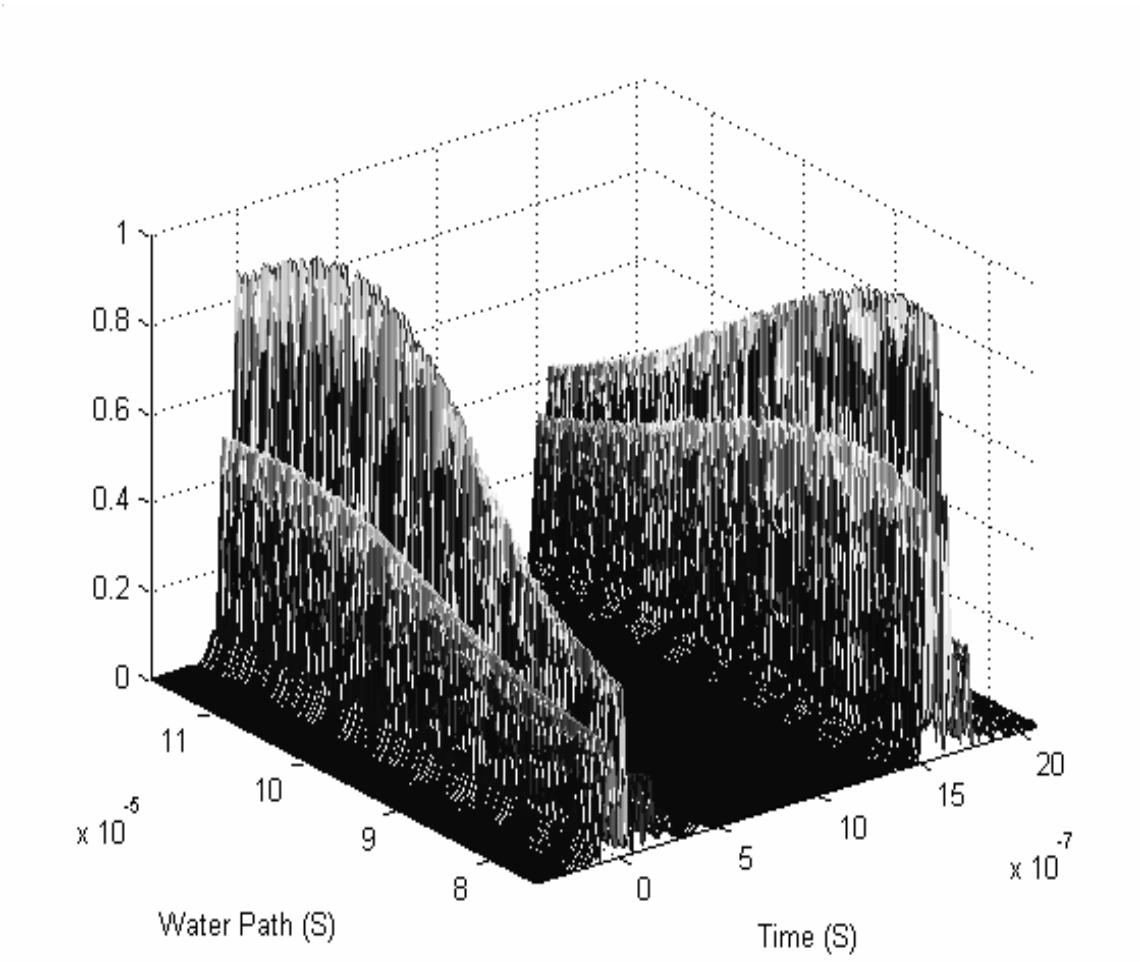

Figure 18: Transducer response (normalized and absolute) as a function of water path and time for the Axial Scan

Finally, the water path times of maximum response were measured and reported in Table 2. The water path times were applied to Equation [12] and subsequently Equation [1] to complete the material characterization. The time domain based thickness and speed of sound propagation estimates along with the error from the classical estimates are reported in Table 3.

Table 2: Water Path and time of maximum response for single z-scan

	Water Path	Time (μs)
FSR	58	104.72
BSR	182	78.978
Delta (Δ)	124	25.745

Table 3: Simultaneous solution estimates for single z-scan

Vs (cm/μs)	Thickness (cm)	Error (%)
0.5952	0.4737	0.260

With the time domain estimation complete, the data analysis was subsequently completed in the frequency domain. The transducer response for all water paths was displayed to confirm that the axial scan included the water paths of maximum response for both the FSR and BSR at each frequency. Observation and calculation of the transducers response shows that while the transmission center frequency was approximately 15 MHz the response was strongest at 9.66 MHz. This reduction in center response frequency was generated by attenuation from sound wave travel through the water and the steel specimen.

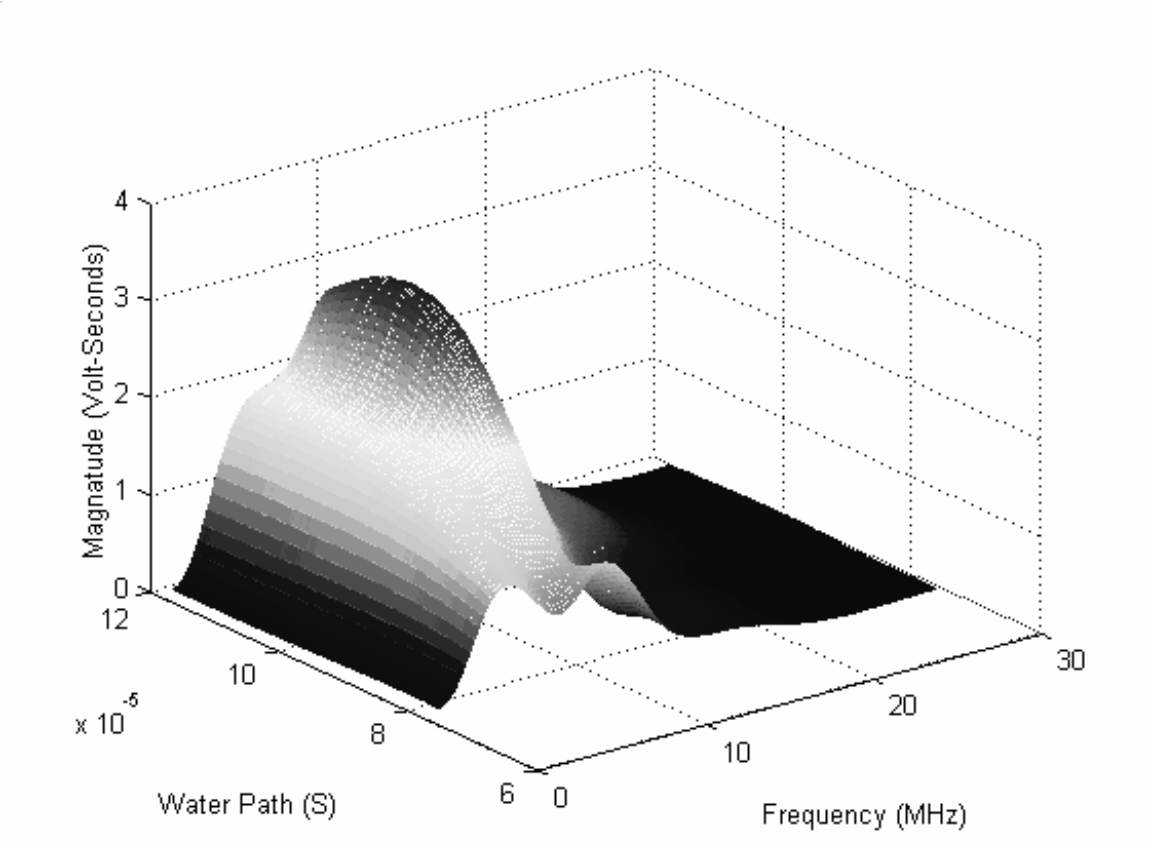

Figure 19: FSR Transducer response (absolute) as a function of water path and frequency for the axial scan

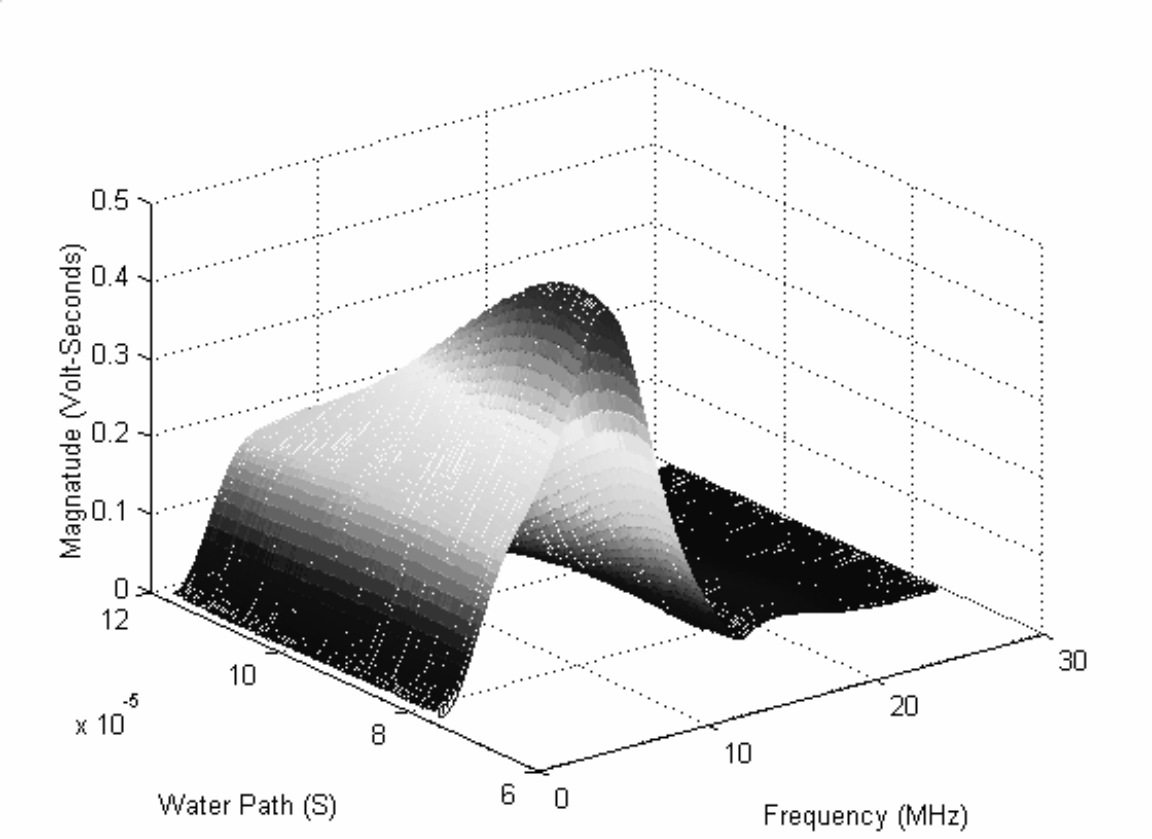

Figure 20: BSR Transducer response (absolute) as a function of water path and frequency for the axial scan

After the adequacy of the scan was confirmed, polynomial curve fits for each frequency in the user selected range across all water paths were completed. The normalized curve fit for the frequency of maximum response is shown with every tenth water path data point in Figure 21. Figure 22 displays the same polynomial curve fits without normalization or the water path data points.

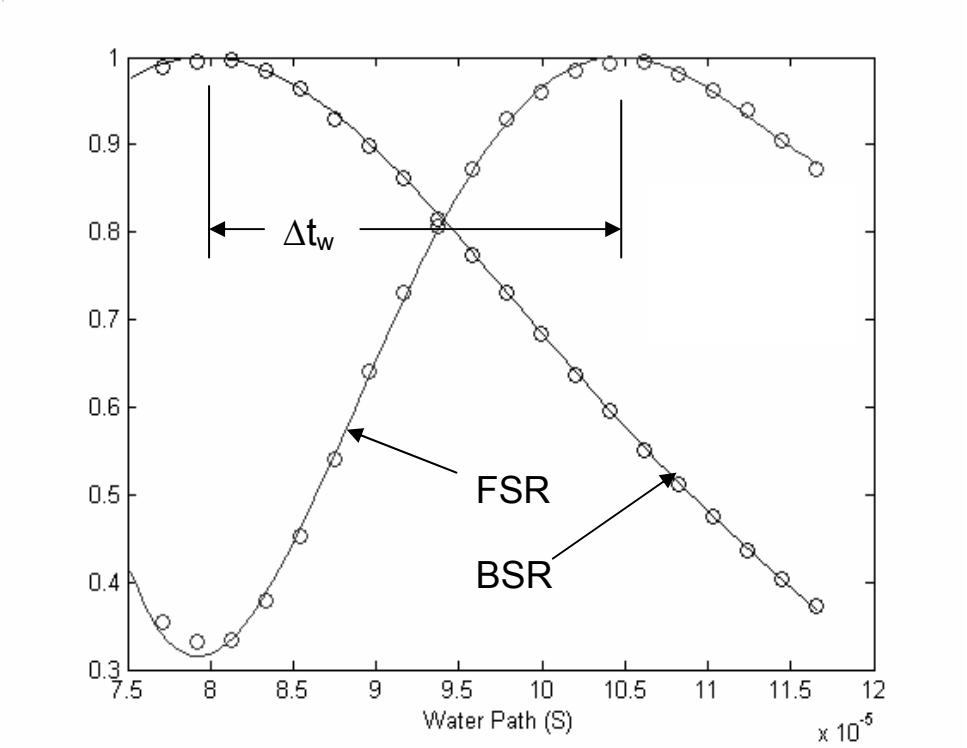

Figure 21: Resulting curve fits through water path data points (every tenth point shown) of the front surface frequency of maximum response (9.66 MHz) for the axial scan

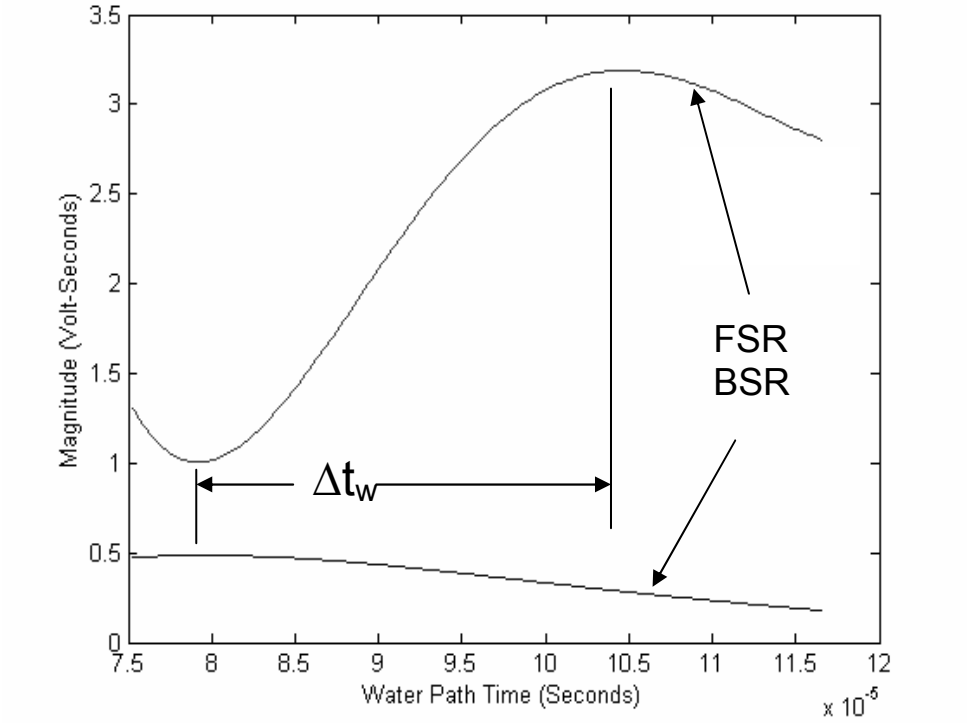

Figure 22: Calculated curves for FSR and BSR at the frequency of maximum front surface response (9.66MHz) for the axial scan

The water path times of maximum response are then interpolated from the curve fits for each frequency in the specified range of interest. The identified water path times are shown for each frequency in Figure 23 and their averages across all frequencies are reported in Table 4.

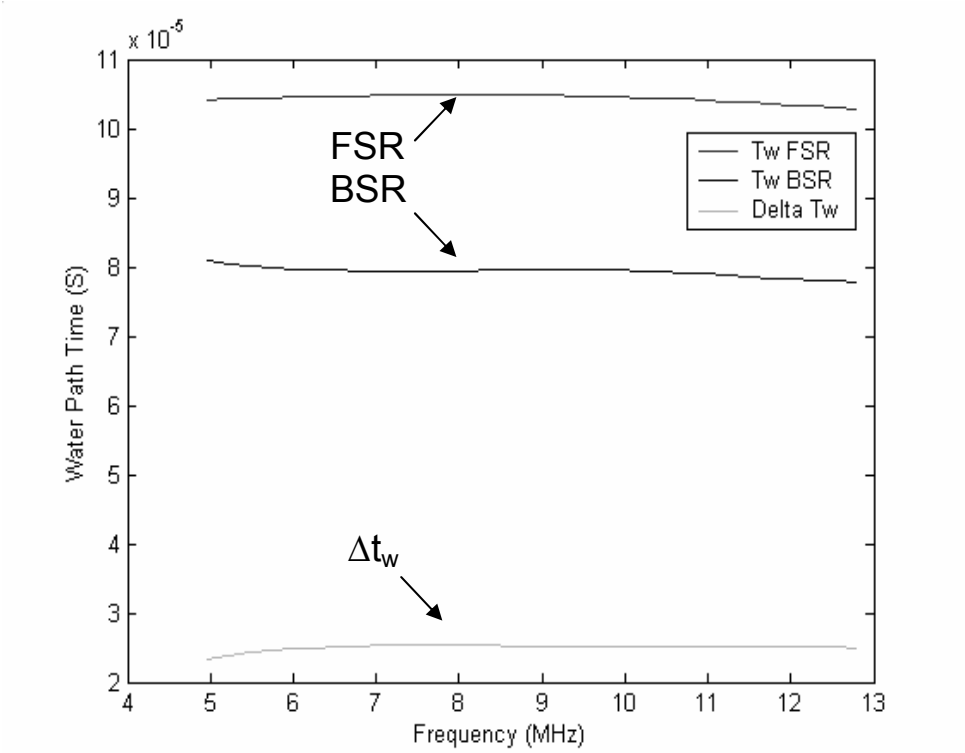

Figure 23: Water path times of maximum response for the axial scan as a function of frequency

Table 4: Average water path times (across frequency) for the single z-scan

	Time (μs)
FSR	104.30
BSR	79.283
Delta (Δ)	25.020

With the water path times and differences calculated a series of velocity of sound propagation estimates are completed. While steel is a non-dispersive material, small errors in data preparation and analysis produce inconsistencies in the velocity estimates. The result is a distribution of velocity estimates whose statistical properties are presented in Table 5 and whose values are shown graphically in Figure 24.

Table 5: Estimated velocity distribution across frequency for the single z-scan

Minimum Vs (cm/μs)	Mean Vs (cm/μs)	Maximum Vs (cm/μs)	Standard Deviation Vs (cm/μs)
0.5672	0.5867	0.5913	0.0052

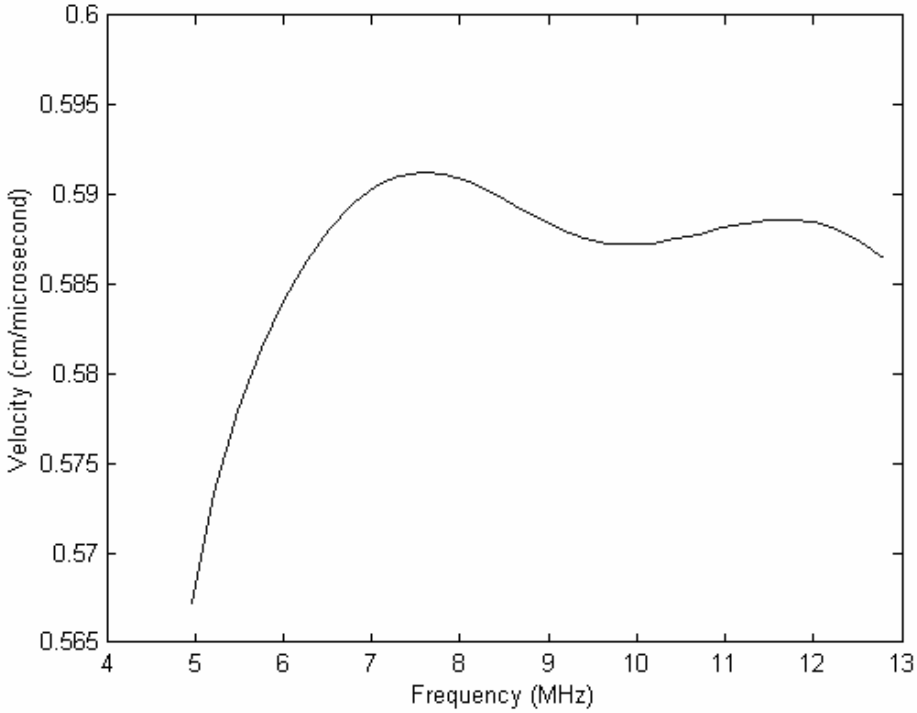

Figure 24: Estimated specimen velocity of sound propagation for the axial scan vs. frequency

Finally, the velocity estimates were averaged across all frequencies and used to calculate the material specimen thickness. The specimen thickness and average velocity estimates are reported in Table 6 along with the percent deviation from the classical estimate.

Table 6: Average estimated thickness and velocity (across frequency) for the single z-scan

Vs (cm/μs)	Thickness (cm)	Error (%)
0.5867	0.4670	1.68

b. Three Dimensional Raster Scan Experiment

This example evaluates the three dimensional raster scan geometry. This scan geometry is useful for evaluating a material specimen over a surface area of interest by providing velocity of sound propagation and thickness measurements as a function of measurement position. The three dimensional raster scan can be used on material specimens of variable thickness or, as this research demonstrates, on specimens of uniform thickness to gain more confidence in the estimates. The material sample in this experiment is a piece of copper with uniform thickness. The results of the preliminary classical velocity of sound propagation and thickness estimates are shown in Table 7.

Table 7: Classical measurement results for the 3 Dimensional raster scan experiment

Thickness (cm)	Δts (μs)	Vs (cm/μs)
0.254	1.1240	0.4520

This scan was completed using the same 15 MHz transducer, 175 water paths and a water path increment of 0.1513 mm. However, instead of completing one measurement at each water path a 5x5 raster of measurements with 1 mm spacing was completed, providing 25 measurement positions at each water path as illustrated previously in Figure 6. For the purposes of data analysis, the resulting data file was treated as 25 unique axial scans.

The data analysis was completed in the same manner as the axial scan example, with the exception that the FSR and BSR matrices had an additional dimension of 25 measurement positions. The signals were prepared in the same manner with the Gaussian multiplier windows being applied as shown in Figure 25. Observation of ratio of the FSR to BSR signal amplitude reveals that while the thickness of the copper sample is less than half that of the previous steel sample, the amplitude is approximately equally attenuated.

While measurement of this characteristic is beyond the scope of this research, it can be inferred that copper is more attenuative than steel.

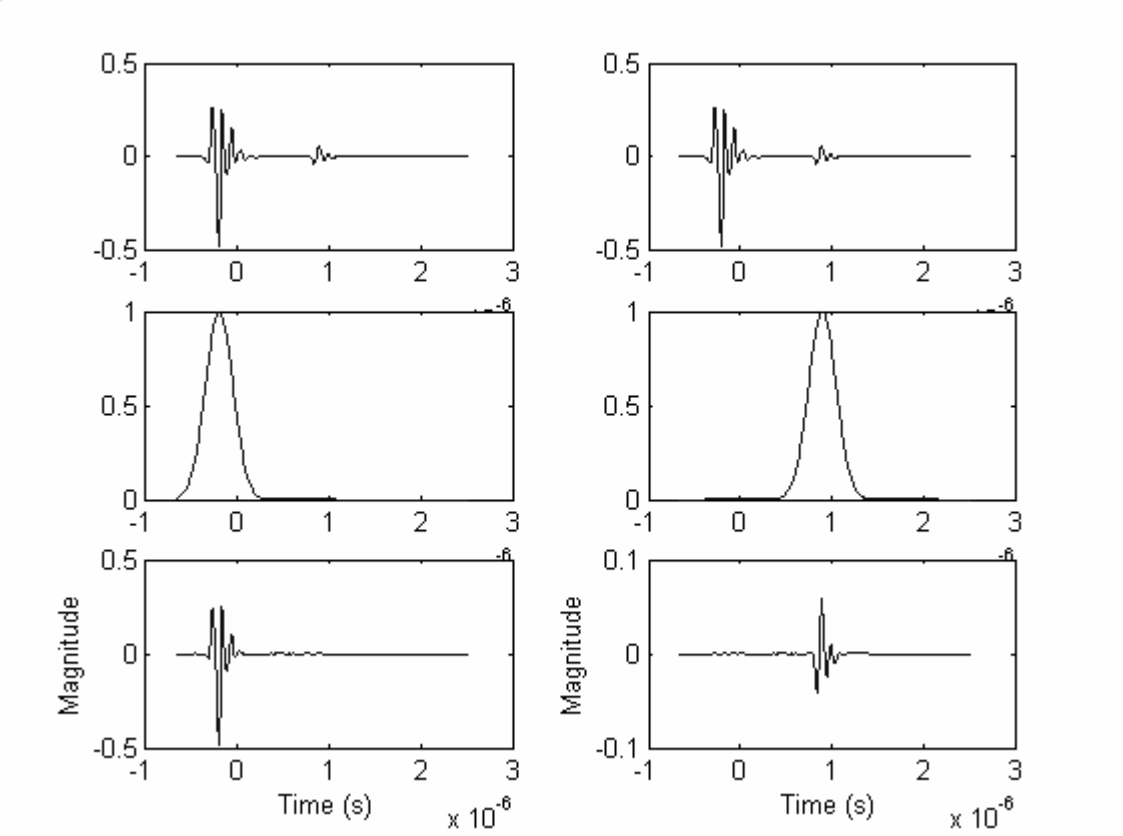

Figure 25: Three-Dimensional Raster Scan rf-signal with Gaussian Multipliers and Resulting Signals (FSR signal on left with BSR on right)

The initial data analysis was completed in the time domain as in the previous example. The resulting normalized absolute transducer response for the first measurement position in the raster is displayed in Figure 26. The response at each of the 25 measurement positions was verified to include the pre-focused FSR to post-focused BSR conditions. Since this material specimen is uniform in thickness, the process of verification for each of the 25 raster positions isn't absolutely necessary, because the specimen and axis of sound propagation were normalized prior to the scan as described earlier, however it is good practice. This is especially true for unknown specimens where this method would be applied.

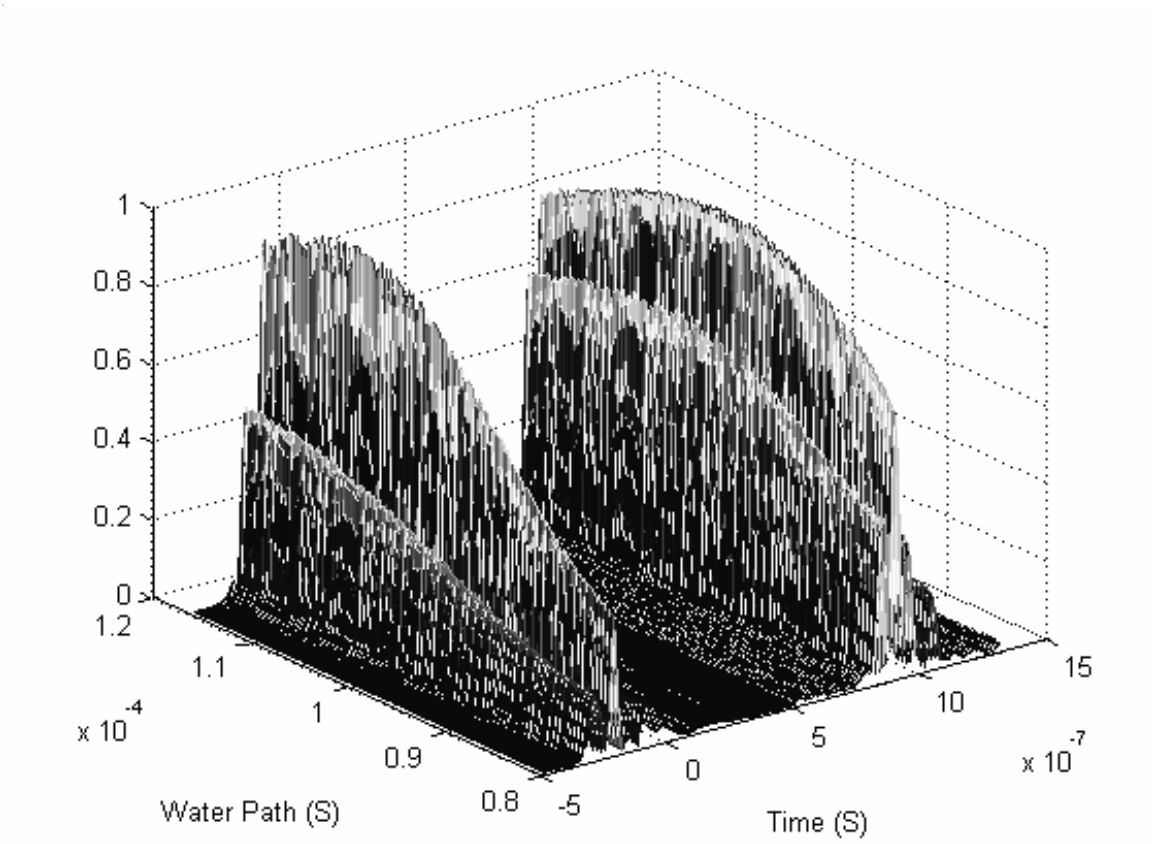

Figure 26: Transducer response (absolute and normalized) as a function of water path and time for the first raster position

To complete the time domain analysis, the water path times of absolute response are identified for both the FSR and BSR at each raster measurement position. This creates distribution of velocity estimates as a function of raster position as displayed in Figure 27 along with the classical estimate and 5% error bars. The distribution of the velocity estimates was evaluated and its statistical characteristics are reported in Table 8.

Table 8: Velocity estimate distribution for all measurement positions

Minimum Vs (cm/μs)	Mean Vs (cm/μs)	Maximum Vs (cm/μs)	Standard Deviation Vs (cm/μs)
0.4146	0.4547	0.4821	0.0190

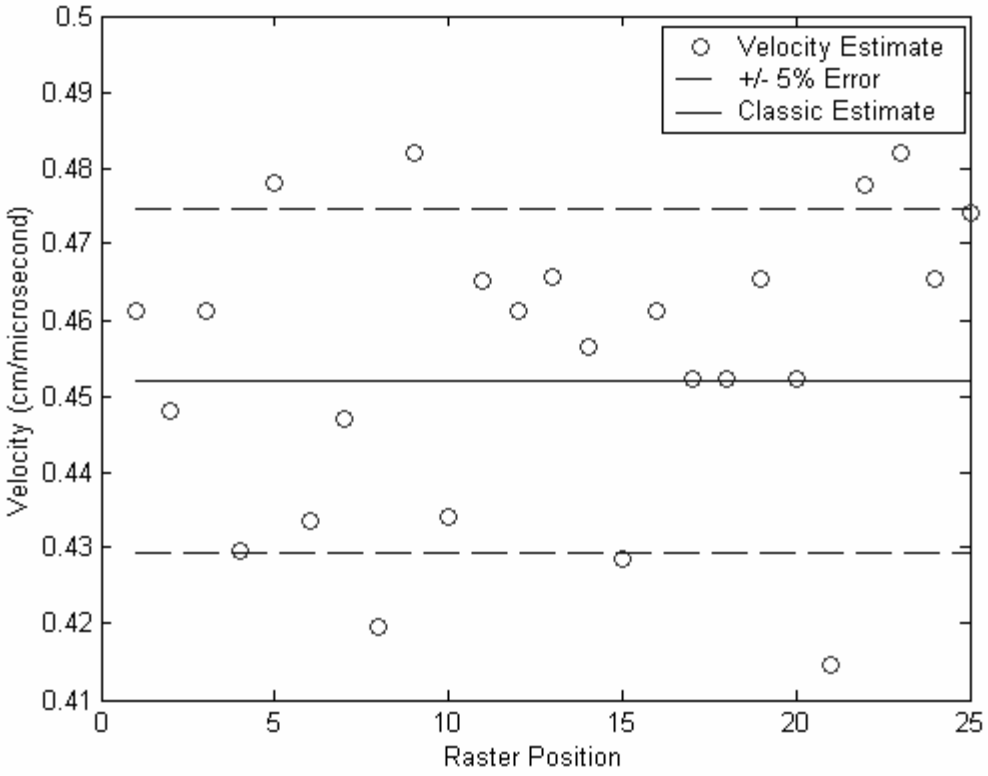

Figure 27: Estimated velocity in the specimen as a function of raster measurement position

Finally, the average thickness and velocity of sound propagation estimate across all measurement positions is reported in Table 9 along with the deviation from the classical estimates. To reduce repetition this is the last experiment that will discuss time domain based estimation in this thesis; however it can be completed in each of the following experiments as well.

Table 9: Average estimates for all measurement positions

Vs (cm/μs)	Thickness (cm)	Error (%)
0.4547	0.2556	0.6130

With the time domain based estimation complete, the analysis was subsequently performed in the frequency domain. As discussed previously, the ultrasonic transducers response was displayed and confirmed to adequately cover both the FSR and BSR water paths of focus for all measurement positions. As shown in Figure 28 and Figure 29, the

scan was started only a few water paths prior to the water path of maximum response for the FSR, however the scan continued for several water paths after the path of interest for the BSR. These extra paths are of no value to this test method. Therefore, if a feedback loop were developed in the data analysis software to eliminate collection of too many water paths, test time and data file size could be reduced.

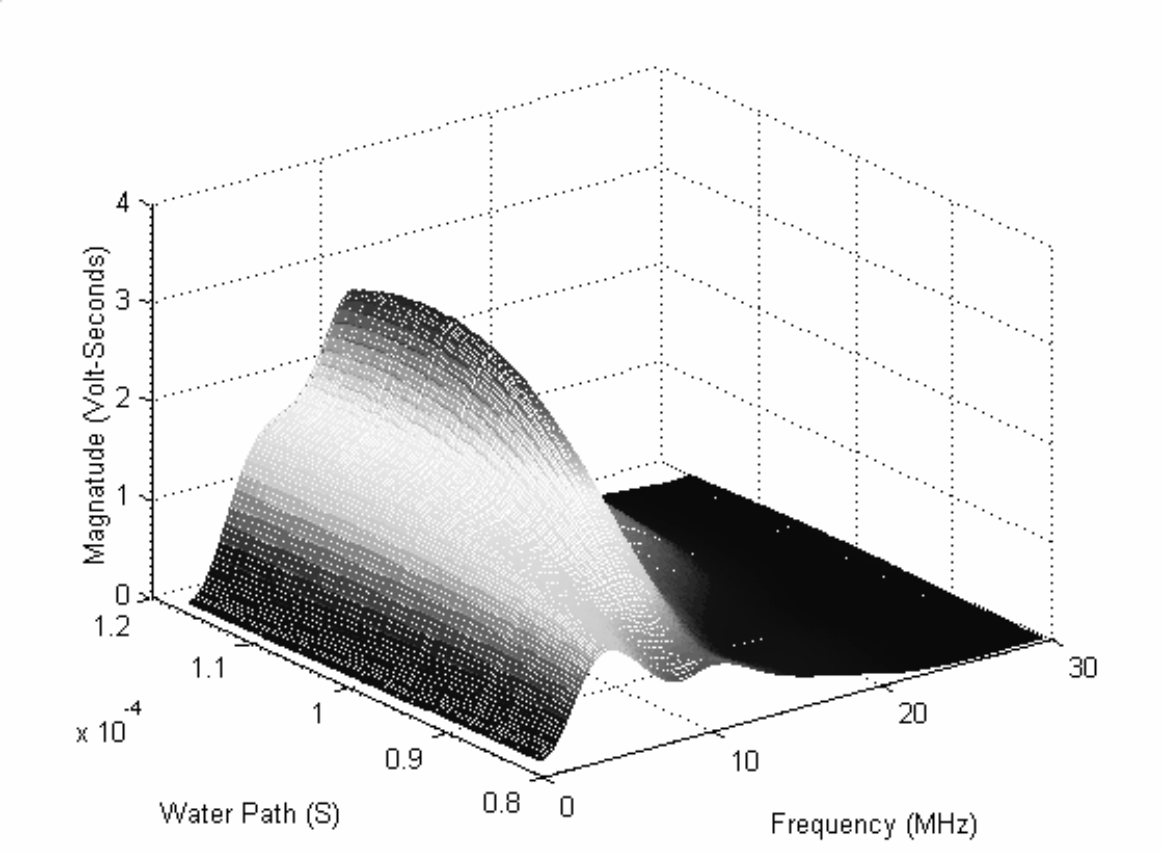

Figure 28: Transducer response (absolute) as a function of water path and frequency for the FSR at the first raster position

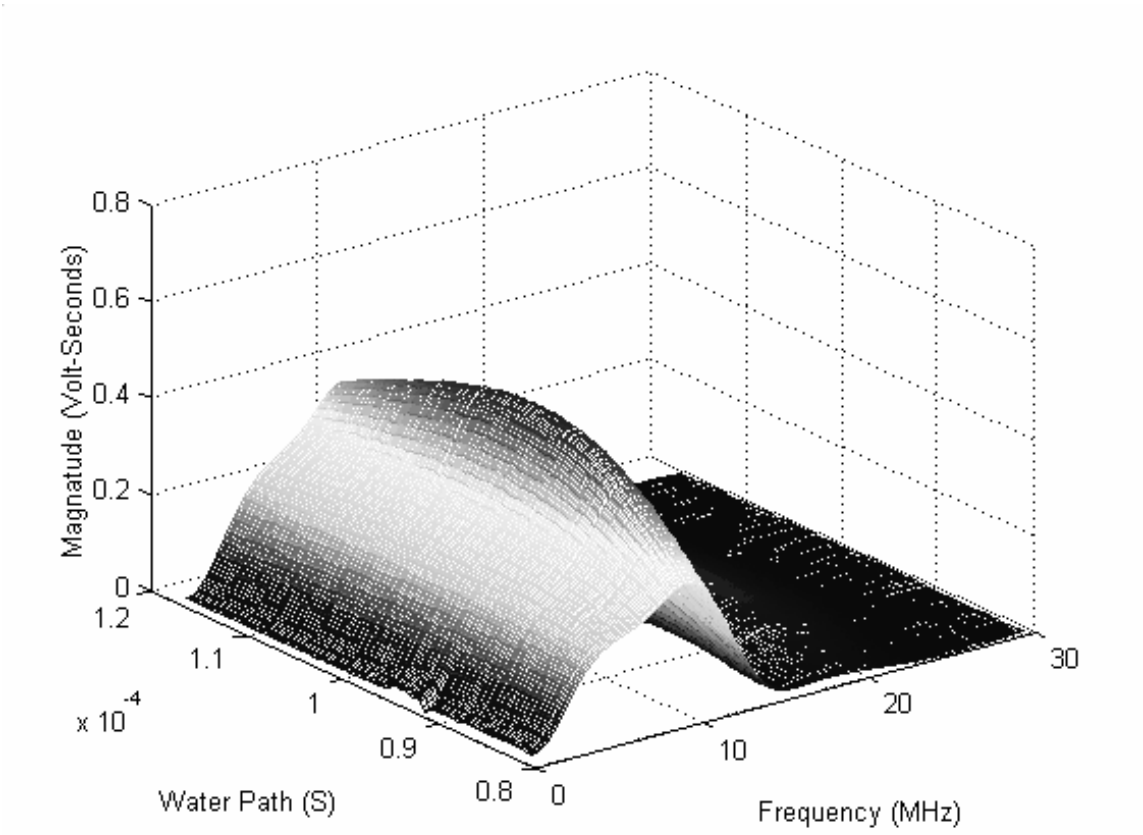

Figure 29: Transducer response (absolute) as a function of water path and frequency for the BSR at the first raster position

As performed in the previous example, polynomial curve fits for each frequency in the user specified range across all water paths were completed for both the FSR and BSR at all measurement positions. An example of the resulting curve fits for the FSR frequency of maximum response at the first raster position is shown in Figure 30. The resulting set of curve fits were used to interpolate between collected water paths and determine a more accurate water path time of maximum response for both the FSR and BSR. The resulting times were averaged across frequency for each measurement position and displayed in Figure 31. Since the material specimen being examined is uniform in thickness, the water path times were averaged again, this time across all measurement positions and reported in Table 10.

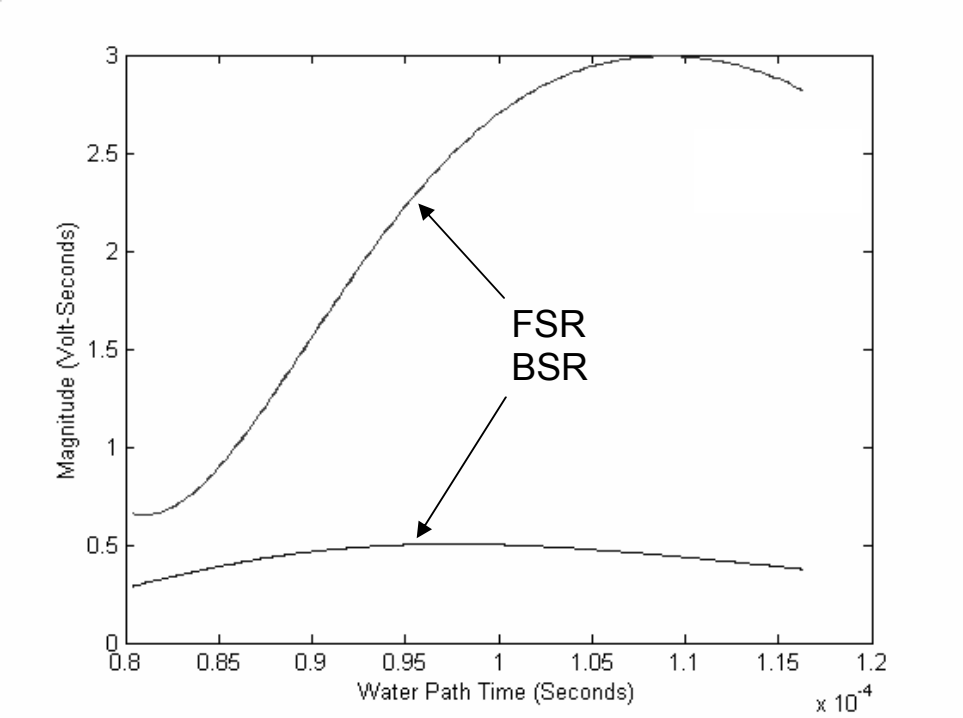

Figure 30: Calculated curves for FSR and BSR at the first raster position and frequency of maximum FSR response

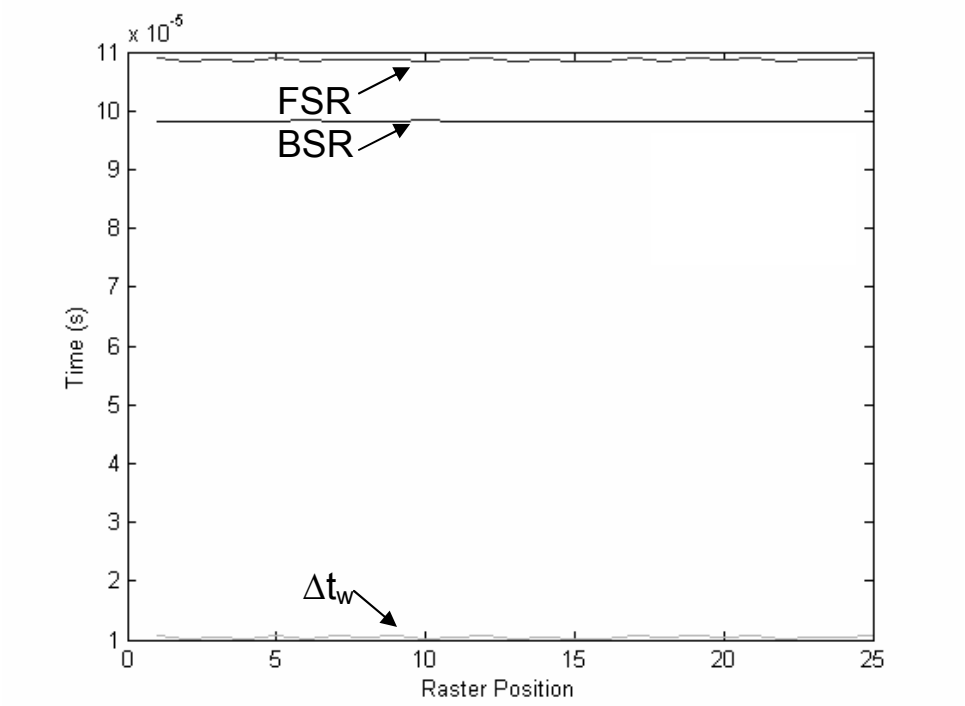

Figure 31: Estimated water path times as a function of measurement position

Table 10: Average water path of maximum response for all frequencies and positions

	Time (μs)
FSR	10.528
BSR	9.5155
Delta (Δ)	1.0127

Using the water path times from the polynomial curve fit maximums and equation [10], velocity of sound propagation estimates are created at each measurement position for each frequency and displayed in Figure 32. The water path times averaged across frequency were then used to create velocity estimates as function of raster position only, and plotted with the classical estimate and 5% error bars in Figure 33. It is interesting to note, that while the measurements as a function of frequency and raster position have a wide distribution as summarized by Table 11, the average estimates across frequency are significantly more consistent.

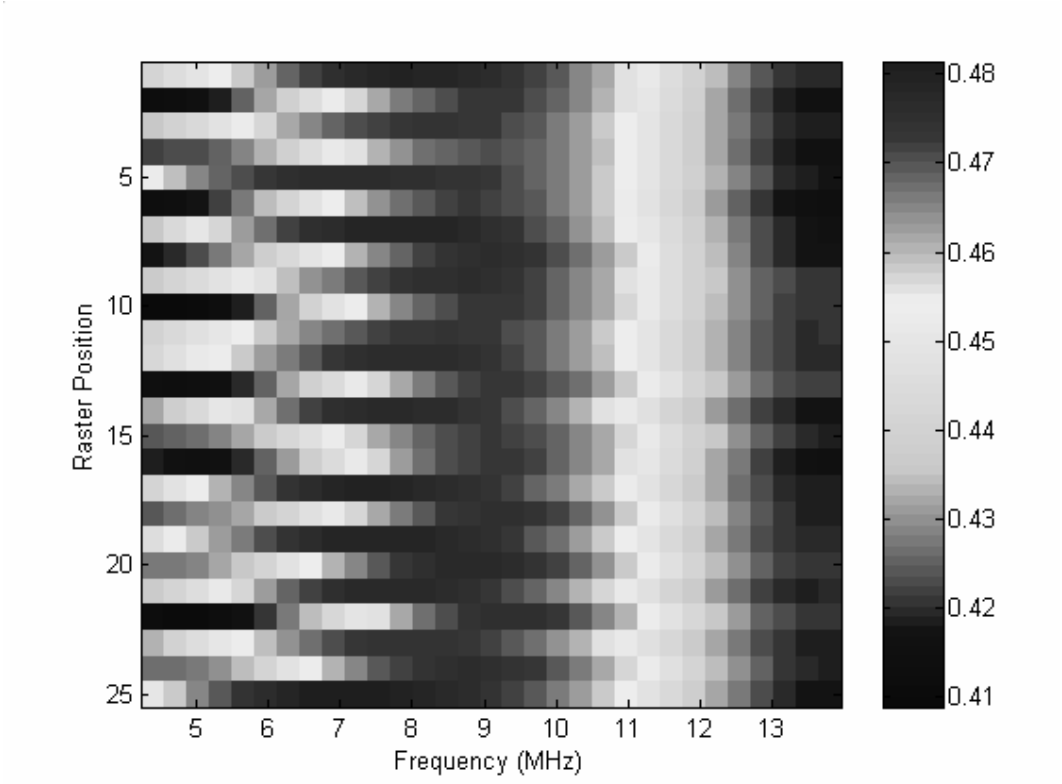

Figure 32: Estimated velocity in the specimen as a function of measurement position and frequency

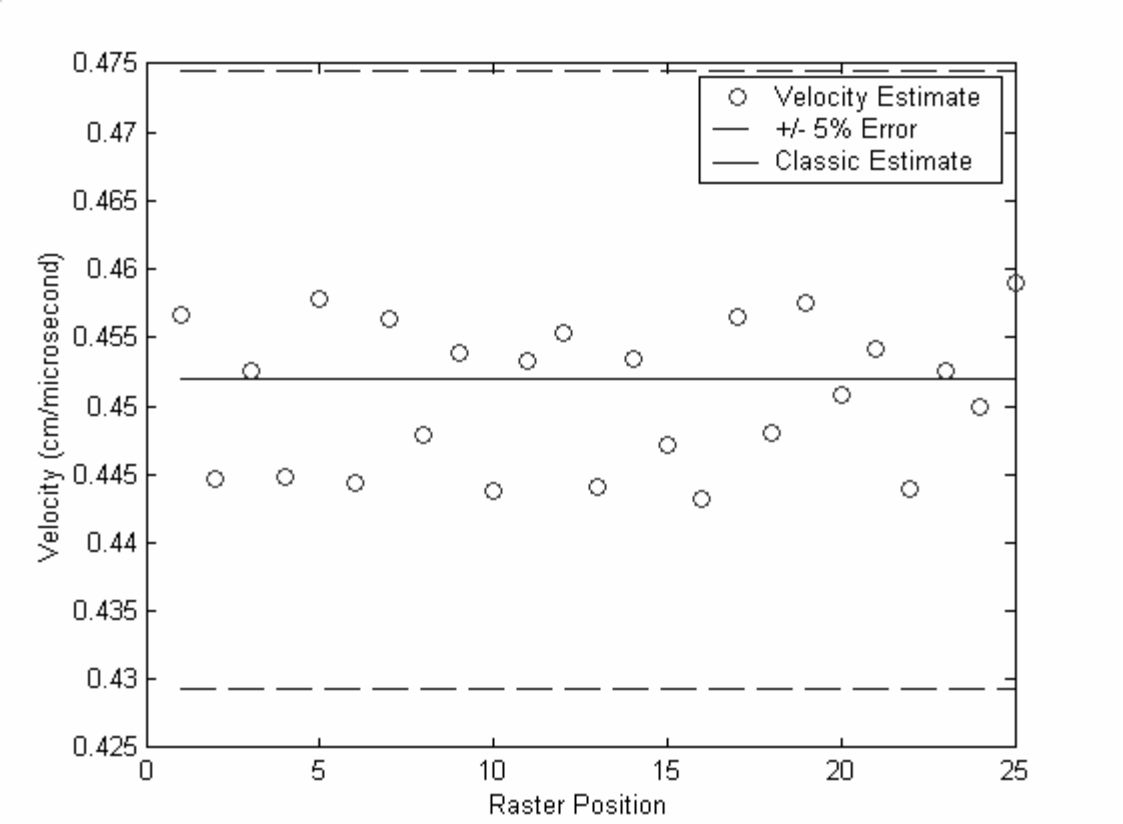

Figure 33: Average velocity (across frequency) in the specimen as a function of measurement position

Table 11: Velocity estimate distribution for a frequencies and measurement positions

Minimum Vs (cm/μs)	Mean Vs (cm/μs)	Maximum Vs (cm/μs)	Standard Deviation Vs (cm/μs)
0.4089	0.4509	0.4815	0.0064

Finally, the average velocity estimate across all frequencies and measurement positions was used in equation [1]. As discussed previously, this is only appropriate for material specimens of constant thickness. The resulting estimate is displayed in Table 12, with the deviation from the classical estimates.

Table 12: Average estimates for all frequencies and measurement positions

Vs (cm/μs)	Thickness (cm)	Error (%)
0.4509	0.2534	0.2382

c. Dual Three Dimensional Raster Scan Experiment

The following experiment presents the dual three dimensional raster scan geometry. As discussed previously, it is important to use properly digitized signals to achieve the best results in data analysis. In the previous examples, the FSR was properly digitized, but the BSR only used a small portion of the available digitization range. The data analysis software was still able to make effective estimates; however, in cases with more extreme sound wave attenuation, the amount of BSR signal available may no longer be adequate.

This experiment used a Beryllium Copper specimen of uniform thickness, whose thickness and classical velocity measurements are reported in Table 13. The two scan geometries were each 75 water paths with 0.1513 mm water path increments. A 5x5 raster at each water path with 1mm spacing between measurement positions completes each scan. The FSR scan originated in the pre-focused FSR state with the pulser receiver gain set to properly digitize the FSR. Once the first scan was completed, the gain was adjusted to properly digitize the BSR. Instead of repeating the same water paths, the second scan originated in the pre-focused BSR position. This reduced the number of water paths that were collected, saving time and reducing file sizes.

Table 13: Classical Measurement Results for the Beryllium Copper Specimen

Thickness (cm)	Δt_s (μs)	Vs (cm/μs)
0.2400	1.012	0.4744

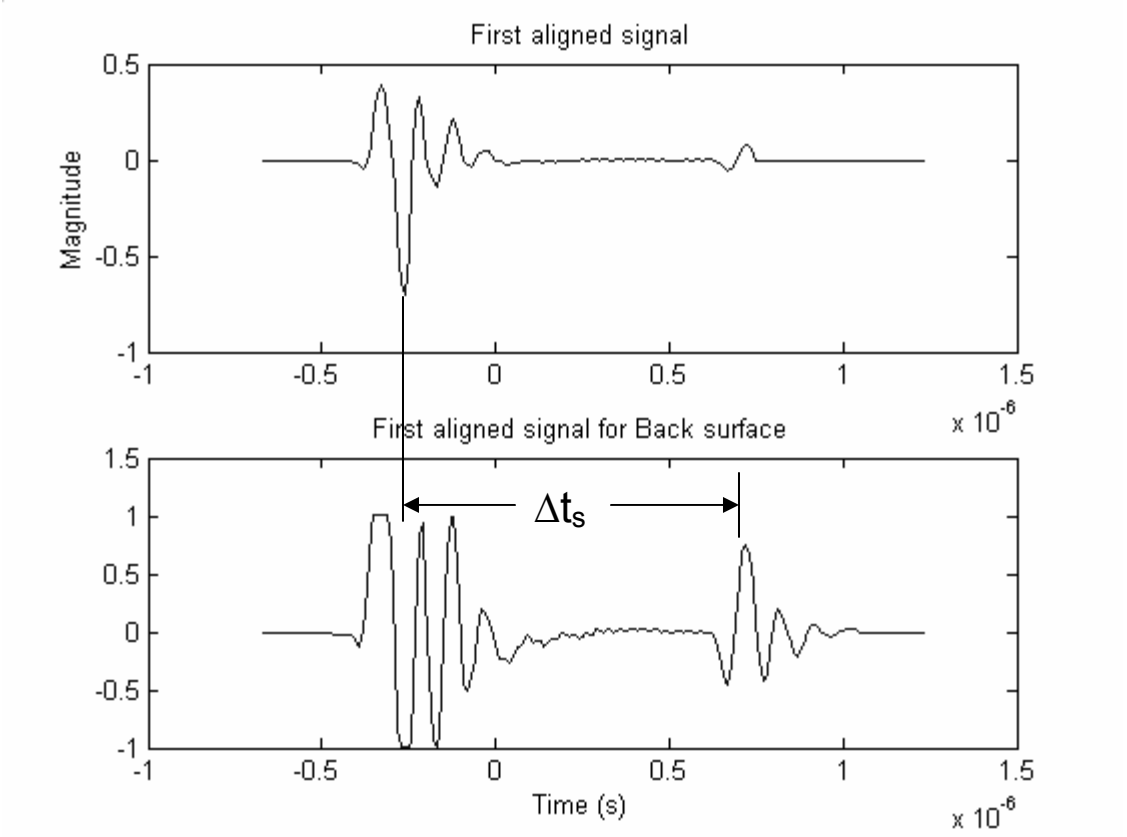

Figure 34: Sample rf-signals generated by the dual 3 Dimensional raster scans

Examples of the resulting signals are shown in Figure 34, with the FSR on top and the BSR scan below. The two scan geometry data analysis is completed in the same way as previous examples, except that the alignment procedure must be competed for each scan within itself and to each other. Once alignment is complete the Gaussian multiplier windows are applied to the appropriate scan data matrix for the correct signal as shown in Figure 35.

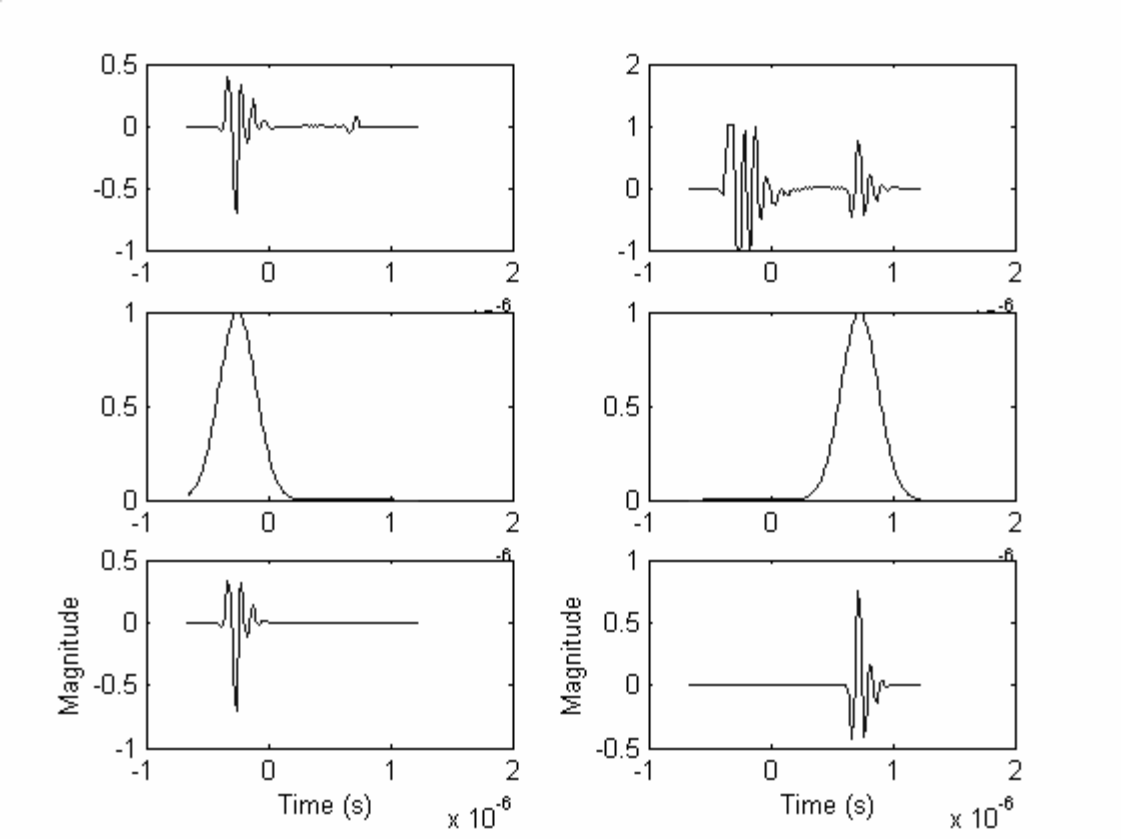

Figure 35: Dual 3D raster scans rf-signals with Gaussian multiplier and resulting signal (FSR raster signal on left with BSR on right)

With the data preparation complete the data analysis was performed. As discussed previously, the analysis is presented only in the frequency domain to reduce repetition. The absolute transducer response for the FSR and BSR at the first raster position is shown in Figure 36 and Figure 37. Once the frequency range of interest is specified by the user, the polynomial curve fits at each frequency are generated. The polynomial curve fits for the frequency of maximum response for the FSR are shown in Figure 38. Notice that the water path times displayed in Figure 36 through Figure 38 do not overlap. Additionally, while the amplitudes of the BSR fits in previous examples (i.e. Figure 30) are significantly lower than the FSR fits, the BSR fit in Figure 38 is actually greater in amplitude due to proper digitization of the waveform.

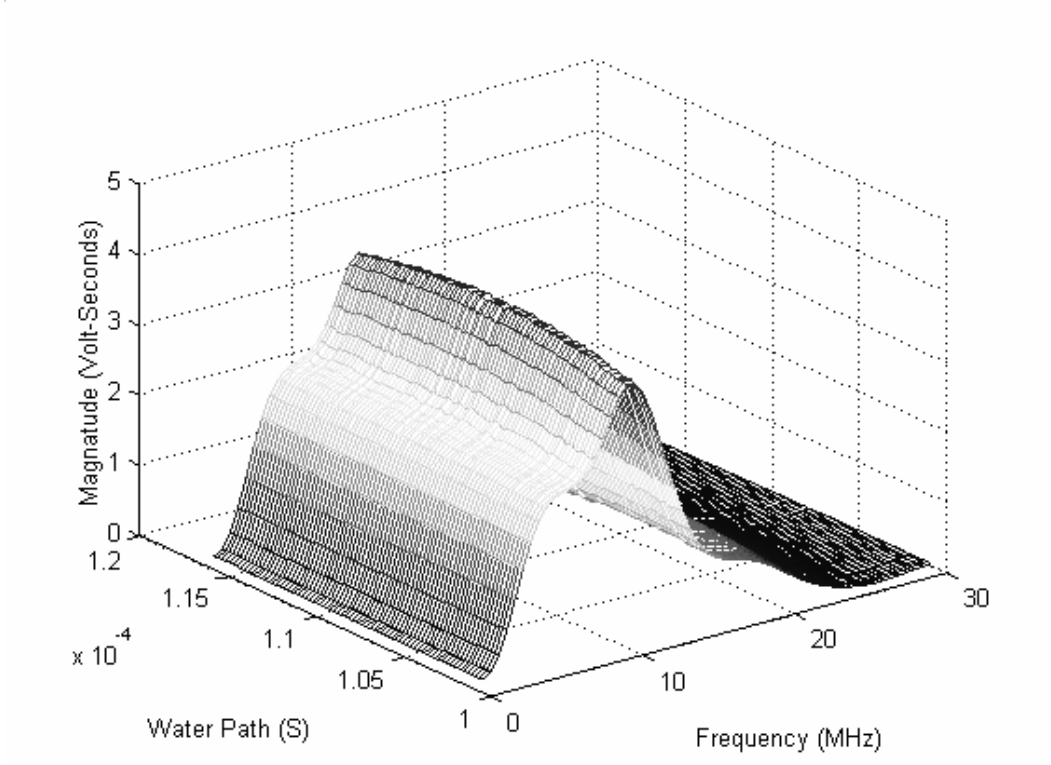

Figure 36: Transducer response (absolute) as a function of water path and frequency for the FSR at the first raster position

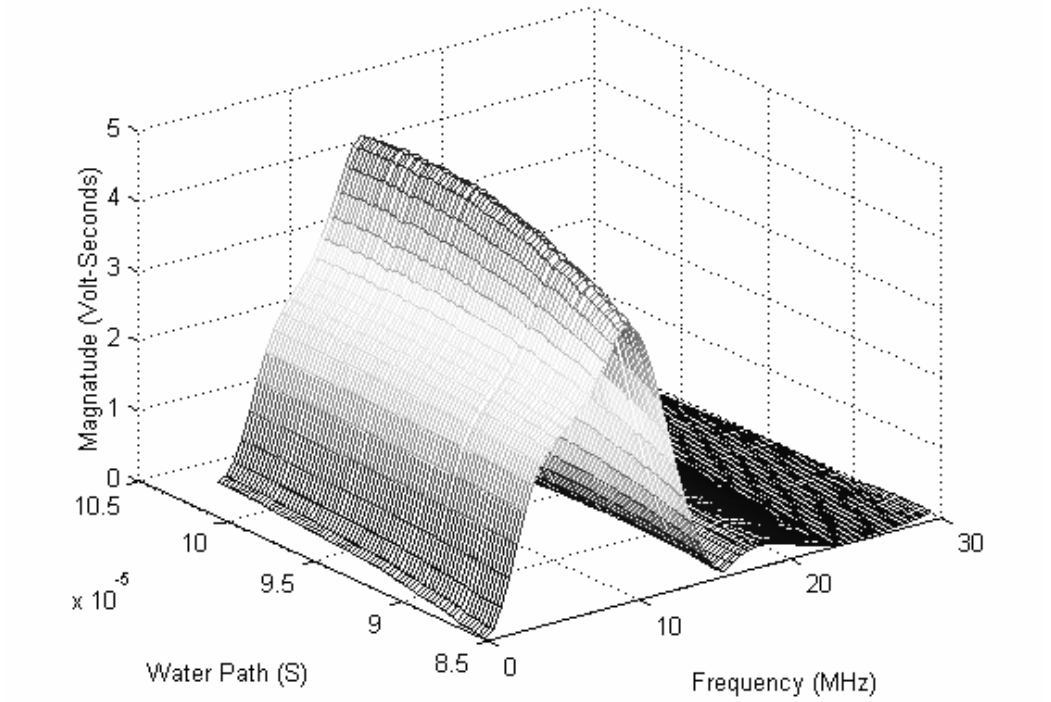

Figure 37: Transducer response (absolute) as a function of water path and frequency for the BSR at the first raster position

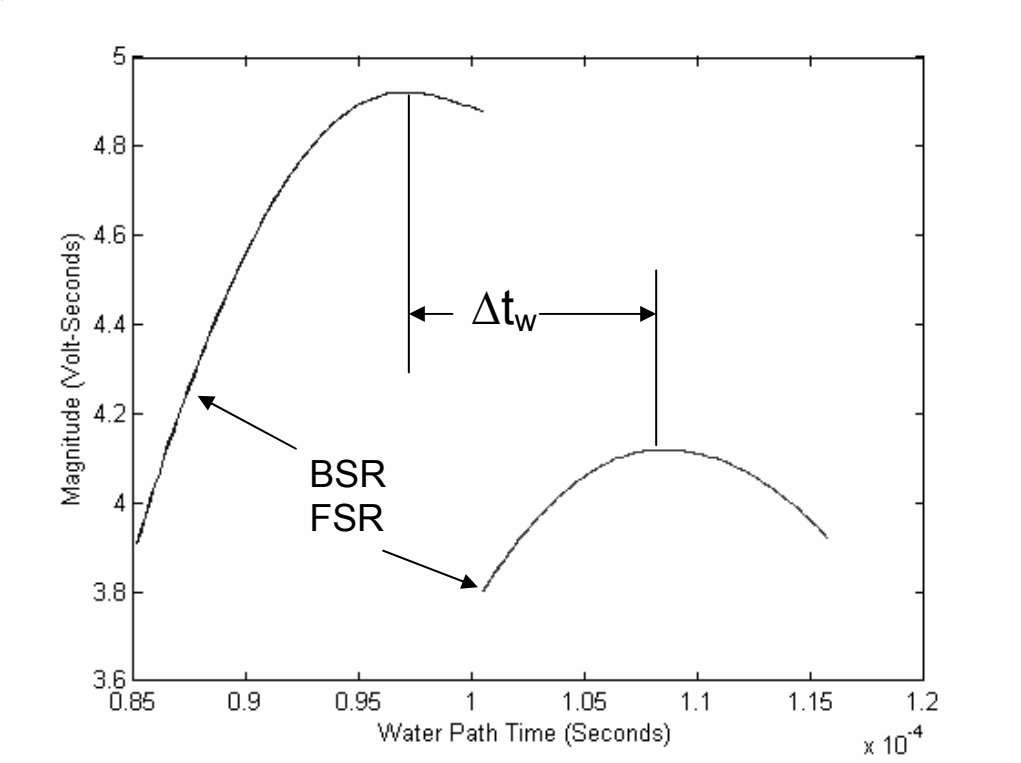

Figure 38: Calculated curves for FSR and BSR at the frequency of maximum front surface response (9.42MHz)

After the curve fits are generated, the water path times of maximum response were calculated. The average water path times across all frequencies for each raster position are displayed graphically in Figure 39. The average times across all frequencies and raster positions are shown in Table 14.

Table 14: Average water path of maximum response for all frequencies and positions

	Time (μs)
FSR	106.652
BSR	96.255
Delta (Δ)	10.427

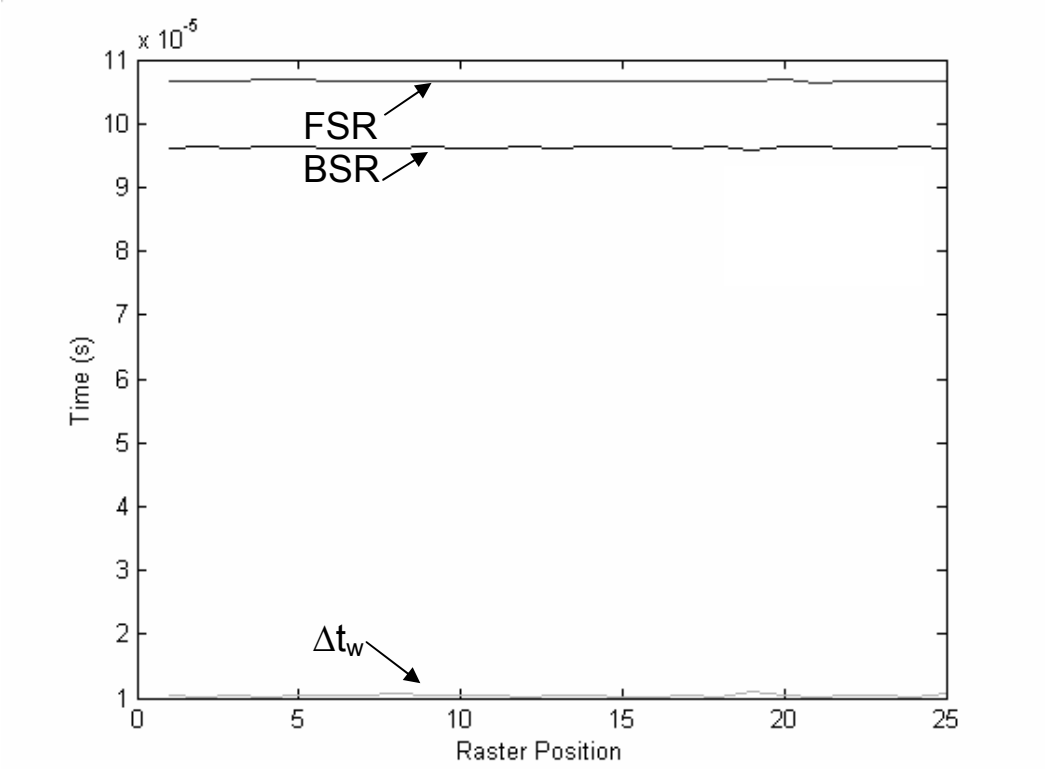

Figure 39: Estimated water path times as a function of measurement position

Finally velocity estimates were calculated at each frequency and raster position as shown in Figure 40. Figure 41 shows the average velocity estimate at each raster position along with the classical estimate and 5% error bars. The average velocity for all raster positions and frequencies along with the thickness estimate and error from the classical estimates is shown in Table 15.

Table 15: Average estimates for all frequencies and measurement positions

Vs (cm/μs)	Thickness (cm)	Error (%)
0.4739	0.2398	0.0900

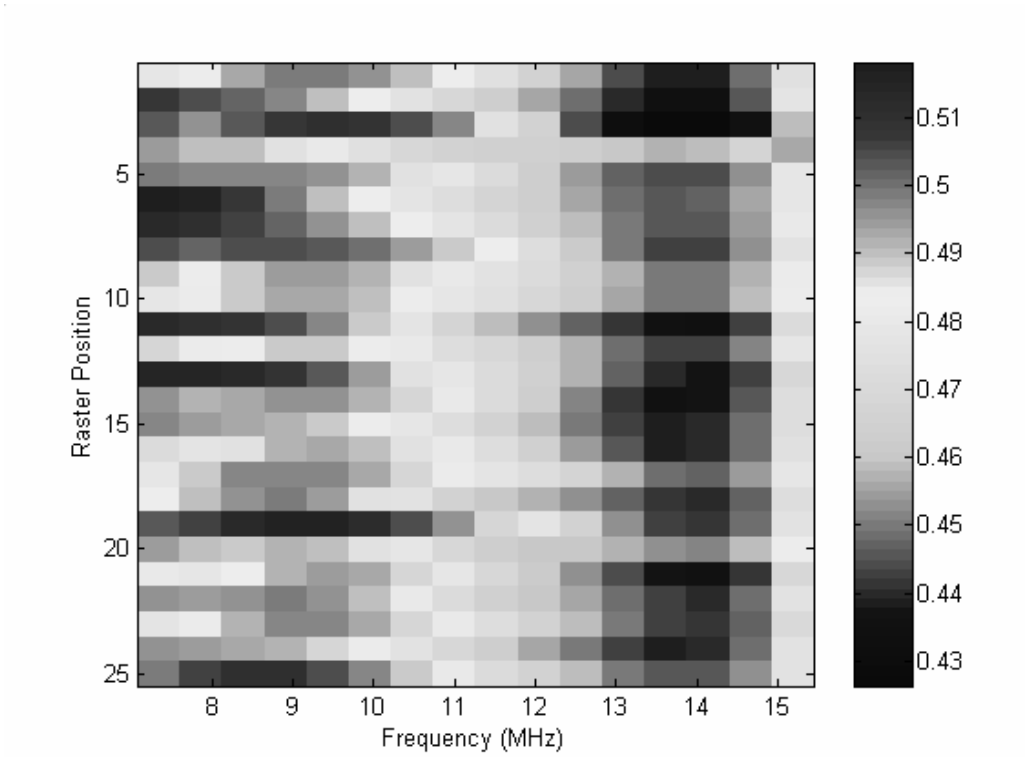

Figure 40: Estimated velocity in the specimen as a function of measurement position and frequency

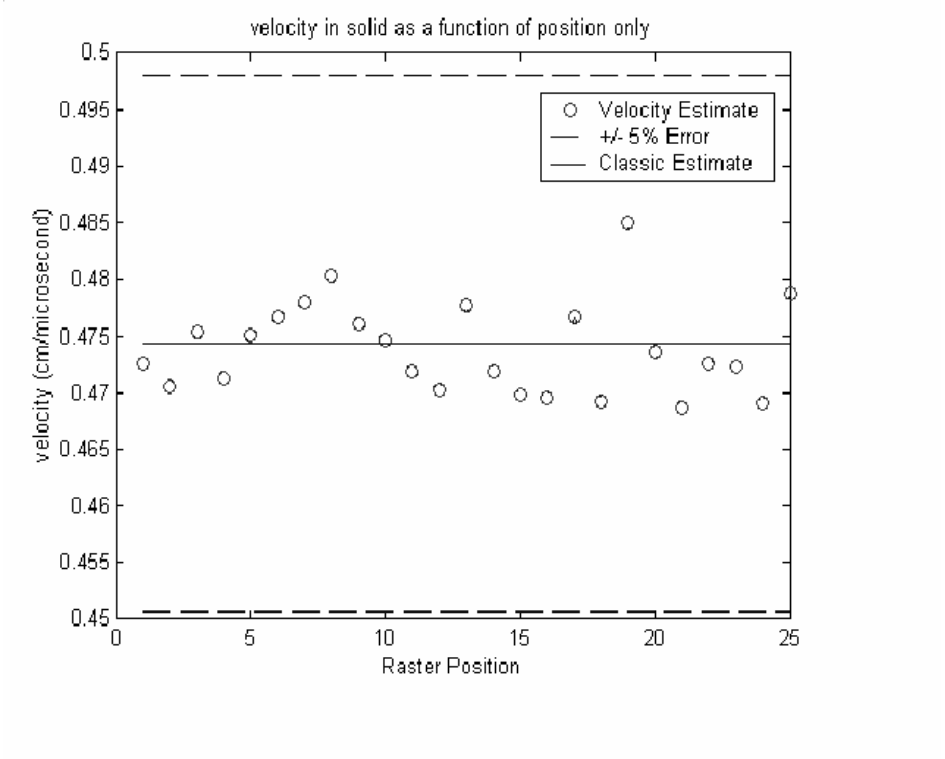

Figure 41: Average velocity (across frequency) in the specimen as a function of measurement position

d. Layered Media

To this point in the thesis, each experiment was performed on the front and back surface reflections of a specimen of uniform thickness. However, this method can be used in more complicated problems for any set of ultrasonic signals, such as subsurface flaw signals or interface signals from layered media. This experiment examines the case of layered media. As discussed in the previous chapter, any layer in the specimen can be inspected without prior knowledge of any other layer in the specimen.

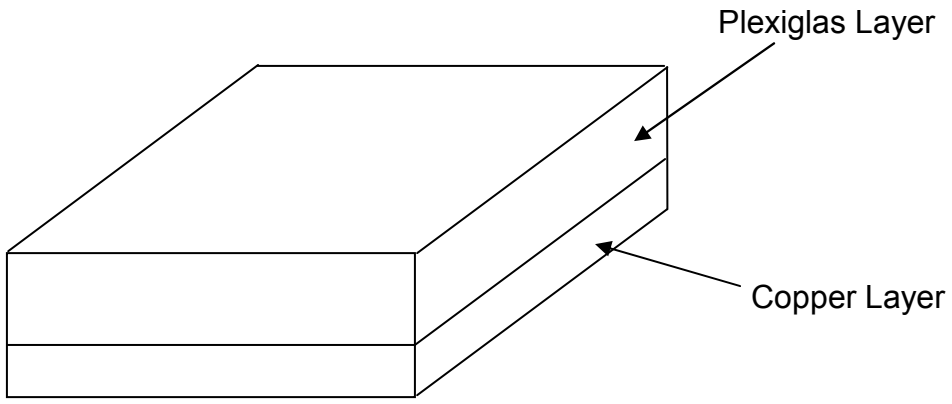

Figure 42: Illustration of Layered Media Specimen

To evaluate this assertion, a two layered specimen was produced with the geometry depicted in Figure 42. Each layer is uniform in thickness. The top layer is Plexiglas and the bottom layer is Copper. Classical velocity and thickness measurements were completed for the Copper layer before the Plexiglas layer was placed on top in intimate contact with the copper layer. While it is possible to complete similar measurements for the Plexiglas layer, none were taken or needed for this evaluation.

Table 16: Classical Measurement Results for the Copper Layer of the Specimen

Thickness (cm)	Δts (μs)	Vs (cm/μs)
0.5334	2.2347	0.4774

With the specimen in place, two 3D raster scans were completed as discussed in the previous example. However, instead of focusing on the FSR during the first scan, the transducer is focused on the interface signal between the Plexiglas and Copper layers. The second scan was completed to focus on the BSR of the Copper layer. Figure 43 is a pair of sample signals. The upper signal is a properly digitized Plexiglas to Copper interface signal and the lower signal is the interface and the properly digitized Copper BSR waveforms. It can be observed, that for the interface waveform scan the Copper BSR signal was not digitized for this experiment.

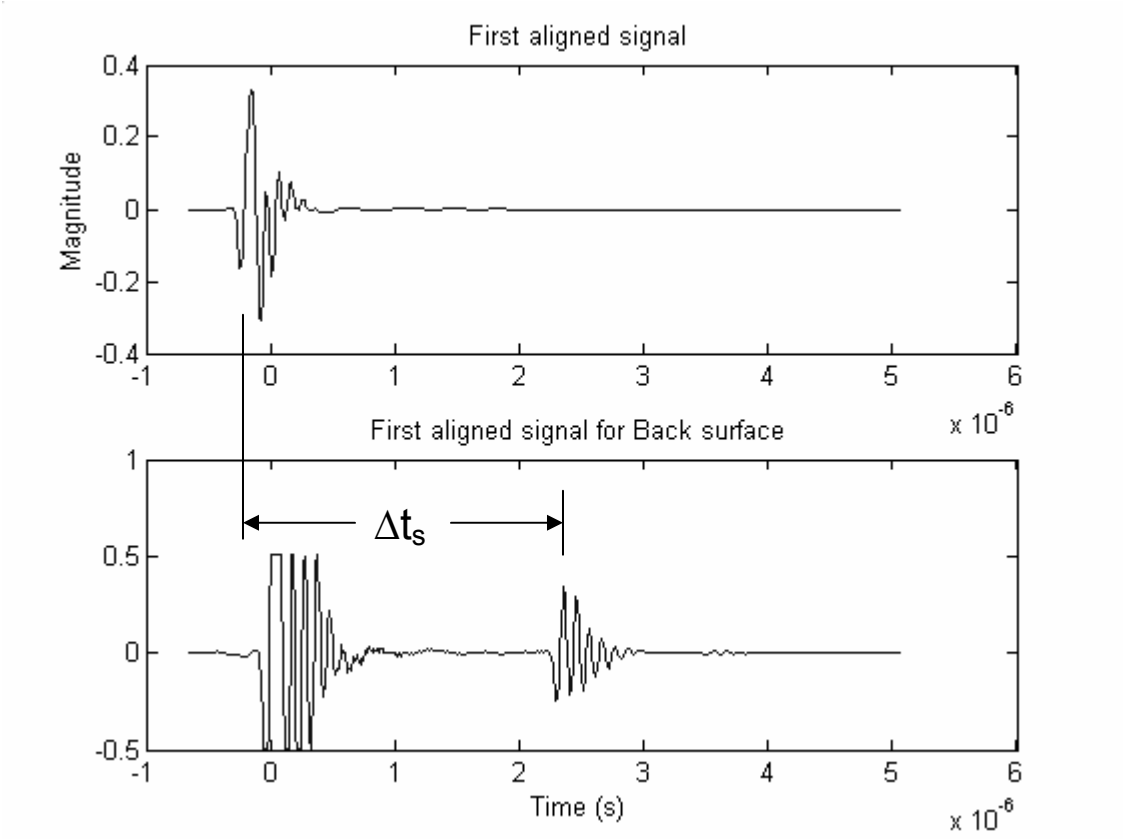

Figure 43: Rf-signals generated by the 3 Dimensional raster scans (layered specimen)

Each three dimensional raster scan consisted of 5x5 raster scans with 1mm spacing at each water path. The scans included 150 water paths with 0.1513mm increments, originating in the pre-focused interface and pre-focused Copper BSR conditions,

respectively. The pulser-receiver gain settings were adjusted to properly digitize the signal of interest in the appropriate scan. Once the scan was complete the signals were aligned and Gaussian multiplier windows were applied as shown in Figure 44.

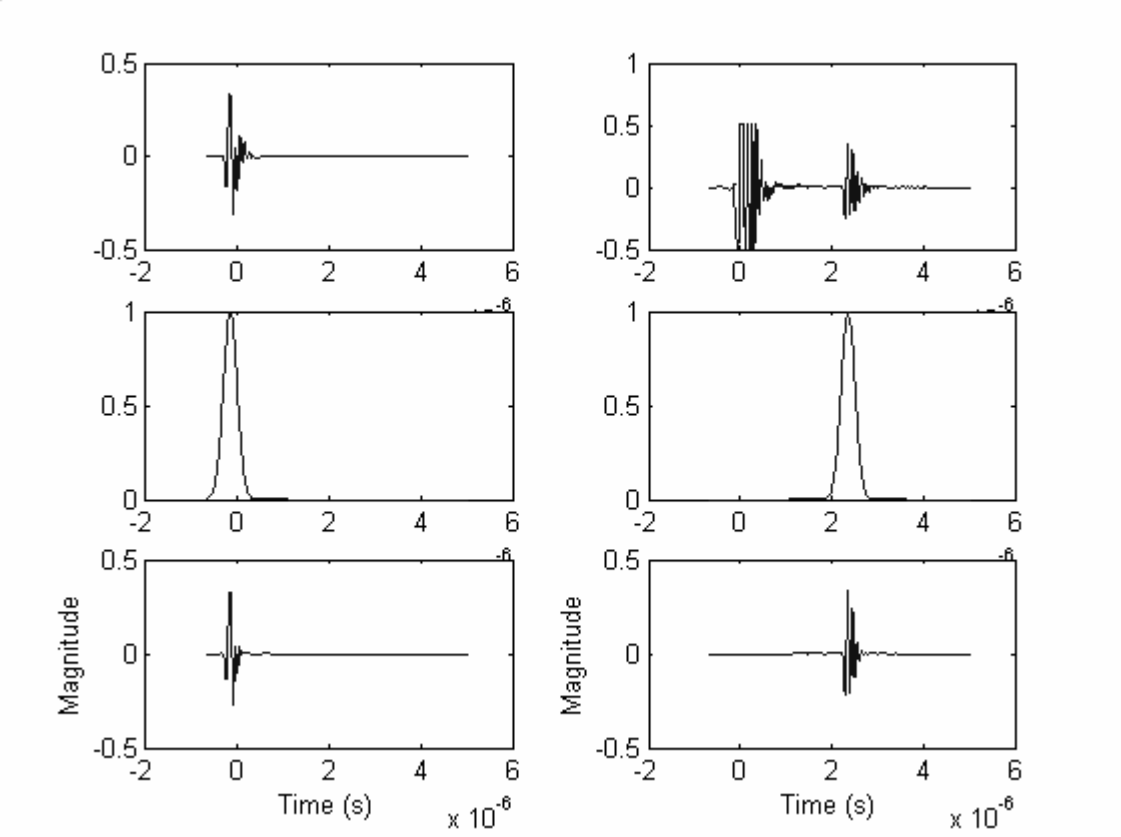

Figure 44: Two layered media scans rf-signals with Gaussian multiplier and resulting signal (interface raster signal on left with BSR of second layer on right)

With the data preparation complete, the transducer response was evaluated, as previously discussed, to ensure the point of maximum response for the signal of interest was captured by the scans. As observed from Figure 45 and Figure 46, the two scans had some overlap of water paths captured in the experiment. Additionally, due to proper digitization of each signal the maximum amplitudes of each scan are roughly equal. While the characterization method is amplitude independent, this is a useful check to confirm consistent digitization methods were used.

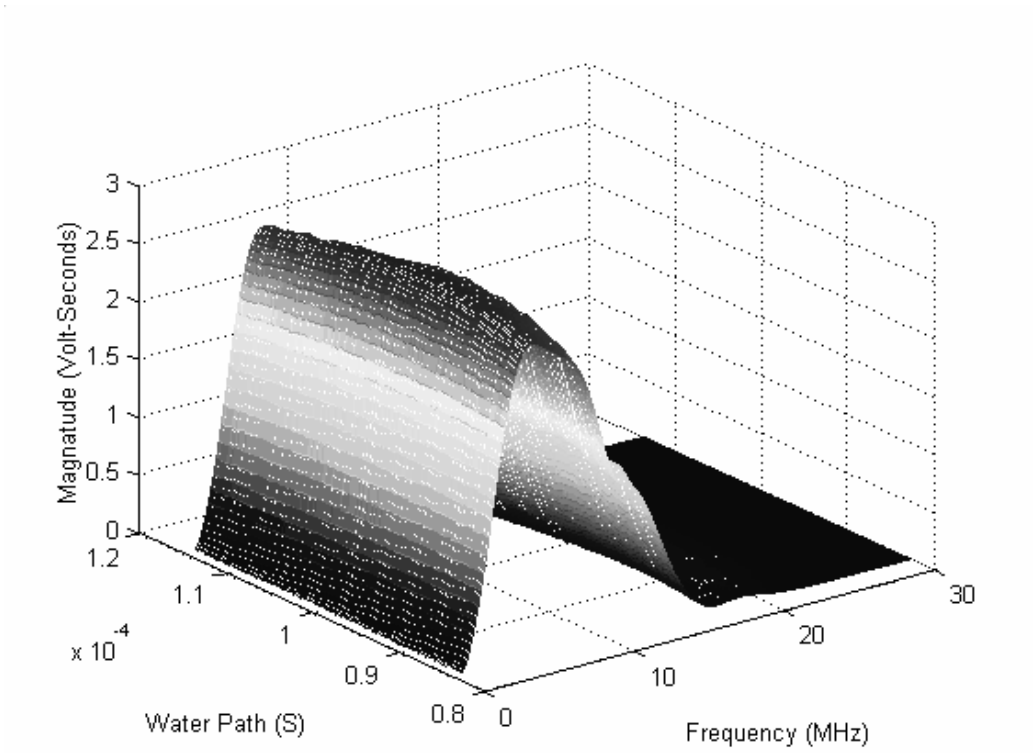

Figure 45: Transducer response (absolute) as a function of water path and frequency for the Interface Signal at the first Raster Position

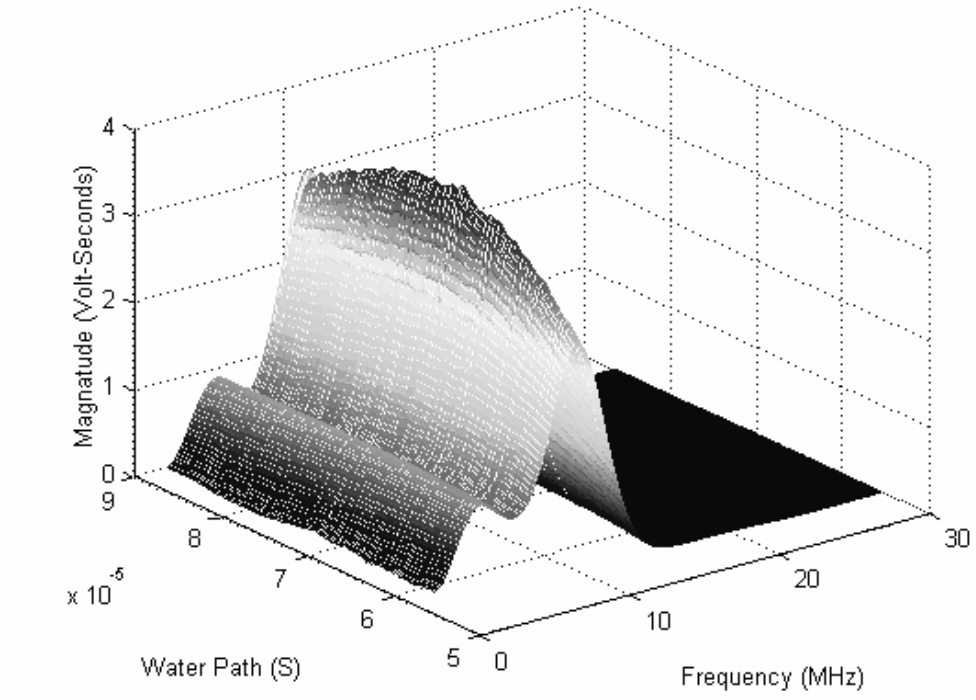

Figure 46: Transducer response (absolute) as a function of water path and frequency for the Copper BSR Signal at the first Raster Position

As performed in each of the previous examples, polynomial curve fits were completed for each scan at each frequency in the user specified range across all water paths. The polynomial curve fits were then used to interpolate the water path times of maximum response at each frequency for all raster positions. The average water path times at each measurement position are displayed in Figure 47 and average times for all frequencies and positions are reported in Table 17.

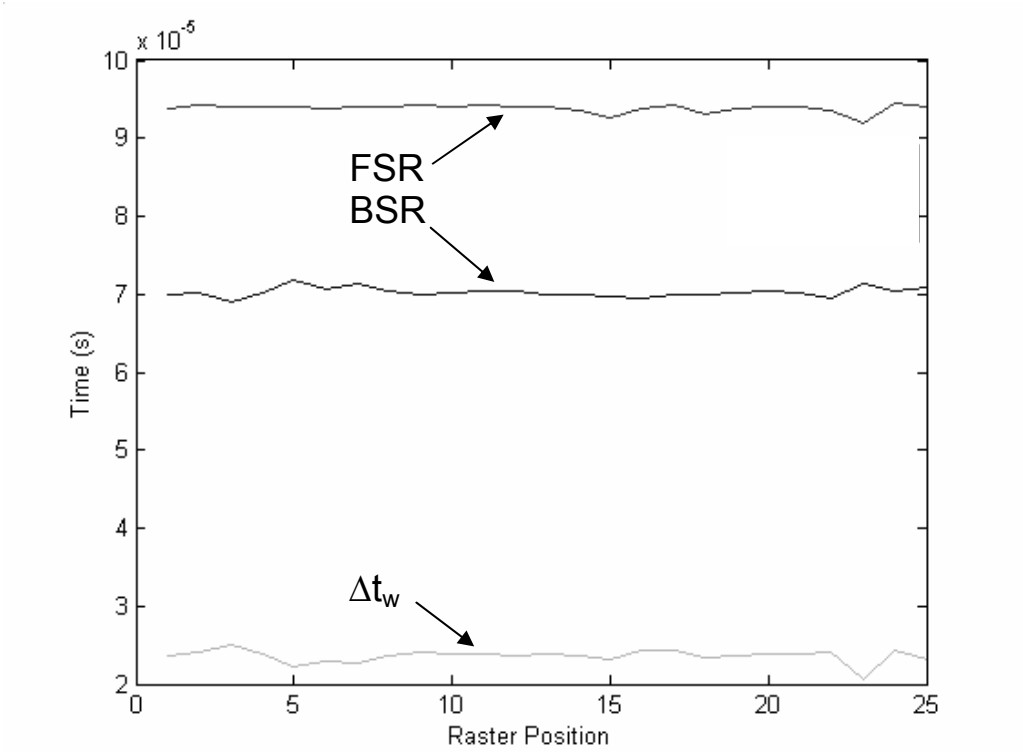

Figure 47: Estimated water path times as a function of measurement position

Table 17: Average water path of maximum response for all frequencies and positions

	Time (μs)
Interface	93.824
BSR	70.251
Delta (Δ)	23.073

The water path times were used to calculate the set of velocity estimates for the Copper layer as a function of frequency and raster position. The estimates are shown in Figure 48. The average velocity of the Copper layer as a function of measurement position is shown in Figure 49 with the classical estimate and 5% error bars. Finally, the thickness of the Copper layer was calculated without any knowledge of the Plexiglas layer and reported with the average velocity in Table 18.

Table 18: Average Estimates of Copper Layer Thickness and Velocity for all Positions and Frequencies (Frequency Domain)

Vs (cm/μs)	Thickness (cm)	Error (%)
0.4772	0.5332	0.0348

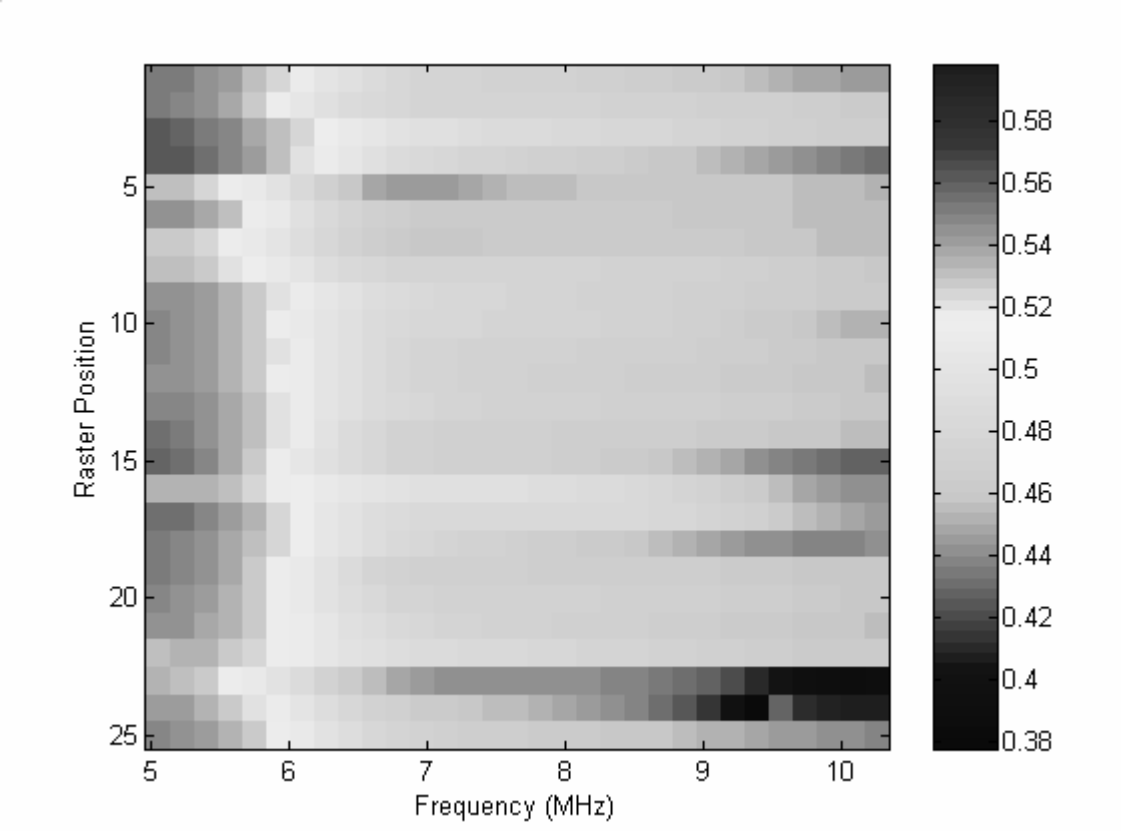

Figure 48: Estimated velocity in the specimen as a function of measurement position and frequency

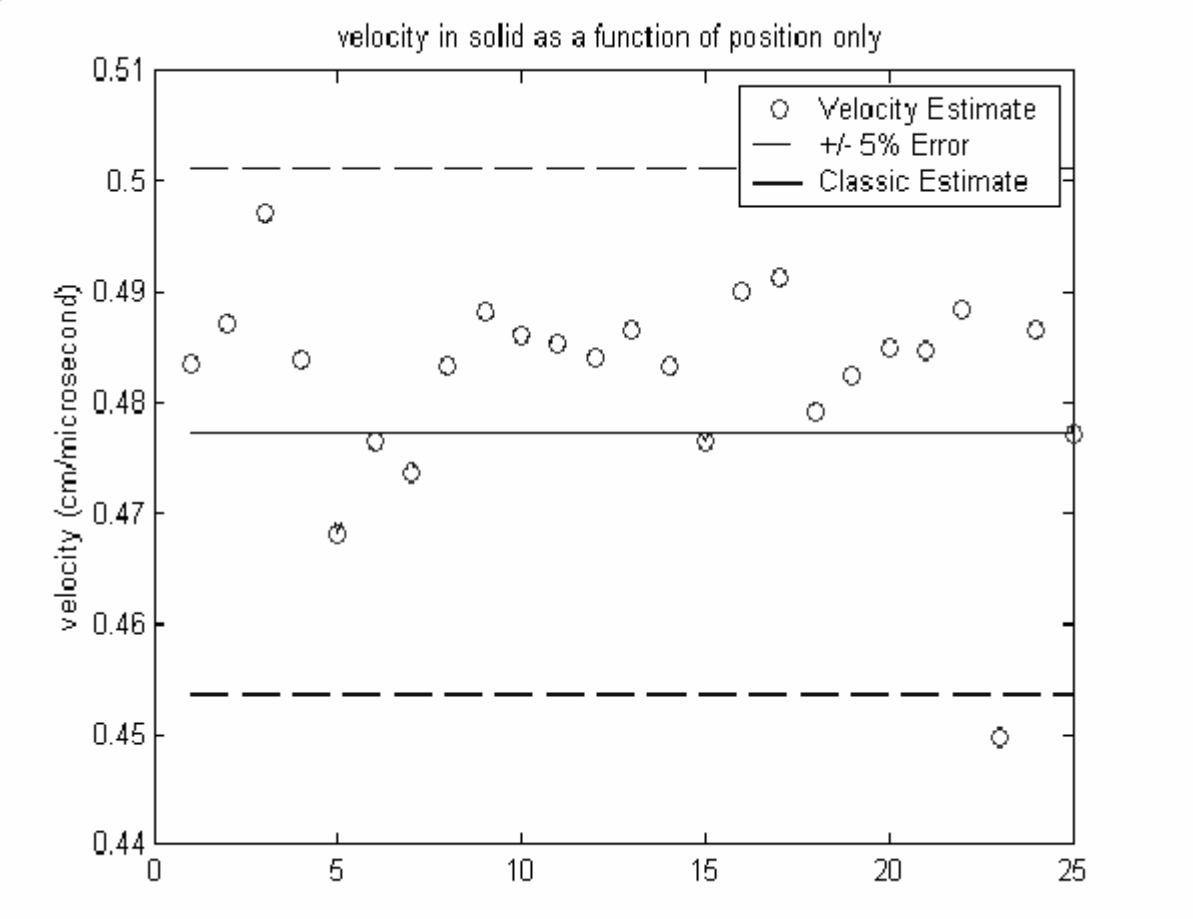

Figure 49: Average velocity (across frequency) in the specimen as a function of measurement position

VI. CONCLUSIONS

The purpose of this research was to investigate the effectiveness of the new test method developed at the University of Missouri-Columbia (MU) as applied to isotropic materials of plate type geometry *Neal* [6.1]. The simultaneous velocity and thickness estimation problem has several existing solutions. However, this new test method is the first to use a single element transducer at normal incidence with only single-sided access to the material specimen.

While the new test method had been previously developed at MU, this was the first research completed to evaluate the method. To perform this evaluation, Matlab programs were developed specifically for this research to perform the data preparation and analysis *Neal* [6.5]. Analysis was completed in the time and frequency domains. The programs are able to complete the analysis for either the axial scan or the three dimensional raster scan geometries. Additionally, the programs are able to use two separate data files for a set of signals to provide the most accurate analysis results by allowing all the waveforms of interest to be properly digitized.

To evaluate the simultaneous velocity and thickness estimation method, four experiments were performed. Each experiment used a different scan geometry or specimen condition providing a unique challenge. The first three experiments were used to characterize unique engineering materials of uniform thickness, employing three different scanning approaches: the axial scan, the three dimensional raster scan, and the dual three dimensional raster scan. Each scanning approach has its own advantages and limitations, but all performed well in estimation of the material specimens characteristics.

The fourth experiment evaluated the method's applicability to layered media and confirmed the ability to characterize a single layer of the media without any prior knowledge or evaluation of the surrounding layers. In each experiment, the new test method provided estimations consistent with the classical velocity and thickness measurements.

These experiments evaluated a variety of scanning configurations, but other challenges still exist. Thus far experiments have been conducted on material specimens where the velocity of propagation is constant for all frequencies. However, this estimation technique and the developed software would also work for dispersive materials, where the speed of sound propagation varies with frequency. Additionally, when the transducer focal length allows, multiple back surface reflections could be used, instead of the front and back surface reflections. The spherically focused ultrasonic transducer could be substituted for a non focused transducer. Finally, in addition to material thickness the test method could be applied to the quantification of the location of flaws or foreign bodies within the unknown media.

Ultimately, this research has shown that while further development of the analysis tools is needed, specifically in the area of frequency range selection, the test method is capable of characterizing the material with no prior knowledge and only single-sided access. Further research will be needed to more thoroughly develop the analysis capability and evaluate the methods applicability to a broader spectrum of materials and geometric challenges. However, the test method has been shown to be an accurate solution to the simultaneous velocity and thickness estimation problem.

REFERENCES

[1.1] Dong Fei, David K. Hsu, and Mark Warchol. Simultaneous Velocity, Thickness and Profile Imaging by Ultrasonic Scan. Journal of NDE. 2002;20(3): 95-112.

[1.2] R. G. Maev and V. M. Levin, Principles of local sound velocity and attenuation measurements using transmission acoustic microscope, IEEE Trans. Ultrason. Ferroelectr. Freq. Control. 1997;44(6):1224-1231

[1.3] Martin E. Anderson and Gregg E. Trehey, The direct estimation of sound speed using pulse-echo ultrasound, J. Acoust. Soc. Am. 1998;104(5):3099-3106.

[1.4] S. Neal, Discussions of simultaneous acoustic velocity and thickness estimates were obtained via private communication with Dr. Steven Neal University of Missouri-Columbia. Columbia, MO 2000.

[2.1] R. Cepel, The Labview data acquisition program used in this work was written by Raina Cepel at the University of Missouri at Columbia. 2000-2001.

[2.2] Ibid

[2.3] Ibid

[2.4] S. Neal, Portions of Matlab code used in this work were written by Dr. Steven Neal at the University of Missouri at Columbia. 1998-2000.

[3.1] R. Cepel, The Labview data acquisition program used in this work was written by Raina Cepel at the University of Missouri at Columbia. 2000-2001.

[4.1] S. Neal, Discussions of simultaneous acoustic velocity and thickness estimates were obtained via private communication with Dr. Steven Neal University of Missouri-Columbia. Columbia, MO 2000.

[4.2] Ibid

[4.3] R. Cepel, The Labview data acquisition program used in this work was written by Raina Cepel at the University of Missouri at Columbia. 2000-2001.

[4.4] S. Neal, Portions of Matlab code used in this work were written by Dr. Steven Neal at the University of Missouri at Columbia. 1998-2000.

[4.5] S. Neal, Discussions of simultaneous acoustic velocity and thickness estimates were obtained via private communication with Dr. Steven Neal University of Missouri-Columbia. Columbia, MO 2000.

[5.1] Ibid

[5.2] S. Neal, Discussions of simultaneous acoustic velocity and thickness estimates were obtained via private communication with Dr. Steven Neal University of Missouri-Columbia. Columbia, MO 2000.

[6.1] Ibid

[6.2] S. Neal, Portions of Matlab code used in this work were written by Dr. Steven Neal at the University of Missouri at Columbia. 1998-2000.

VITA

Brett Andrew Rinker was born February 3, 1976 in Tacoma, Washington. After attending public schools in Missouri, he received the following degrees from the University of Missouri-Columbia: Bachelors of Science in Mechanical and Aerospace Engineering (1999); and Masters of Science in Mechanical and Aerospace Engineering (2006). He has been employed as a Nondestructive Testing and Product Engineer at Honeywell Federal Manufacturing and Technologies since 2001. Brett is married to Theresa Susan Rinker M.D., the former Theresa Sudholt.